UNIVERSIDAD DE SANTIAGO DE CHILE

FACULTAD DE CIENCIA

Departamento de Física

Out of equilibrium dynamics in spin chains

Lautaro Lucas Gabriel Labarca Guajardo

Profesor Guía:

Guillermo Romero Huenchuñir

Tesis para optar al grado académico de Magíster en Ciencias con Mención en Física

Santiago - Chile

2021

FONDECYT – 1190727 – Circuit quantum electrodynamics for nonequilibrium physics of few- and many-body systems.

Resumen

En este trabajo, estudiamos la dinámica fuera del equilibrio de una cadena de spin-1 siguiendo un protocolo de quantum quench. El modelo en específico estudiado es una cadena XY-spin-1 con anisotropía. Estudiamos las escalas de tiempo relevantes y la evolución del Loschmidt echo, observables y entropías bipartitas. Exploramos posibles parámetros de orden para caracterizar la dinámica, y el rol de la simetría de paridad del modelo en la distribución de la información mutua. Identificamos con éxito parámetros de orden adecuados para caracterizar la dinámica emergente. Adicionalmente, brindamos una introducción pedagógica a conceptos centrales de la teoría de información clásica y cuántica, tales como la entropía de Shannon, información mutua y quantum discord.

Palabras clave: Protocolo de quench, cadena de spin-1 no integrable, transición de fase dinámica cuántica, información cuántica.

Abstract

In this work, we study the out of equilibrium dynamics of a in general non-solvable finite spin-1 chain following a protocol of quantum quench. The specific model studied is the XY-spin-1 chain with single-ion anisotropy. We study the relevant time scales and the evolution of Loschmidt echo, observables and bipartite entropies. We identify signatures of a dynamical quantum phase transition. We also explore possible order parameters for characterizing the dynamics, and the role of the models parity symmetry on the mutual information distribution. We succeeded in identifying adequate order parameters characterizing the emerging dynamics. Additionally, we give a pedagogical introduction to central concepts of classical and quantum information theory, such as the Shannon entropy, mutual information and quantum discord.

Keywords: quench protocol, non-integrable spin 1 chain, dynamical quantum phase transitions, quantum information.

Acknowledgments

I thank the financial support of FONDECYT 1197027. I also thank the Science Faculty of the Universidad de Santiago de Chile for the given scholarship that made possible this work.

I want to thank my Professor, Dr. Guillermo Romero, for his support and patience throughout the development of this work. I extend this gratitude to Dr. Sebastián Allende and Dr. Juan Carlos Retamal for their support, insightful comments and constructive criticisms. I also thank the PhD student Rubén Peña for his initial support.

Finally, I want to thank all the administration workers at the Science Faculty that make possible our scientific work.

Contents

List of Figures

Chapter 1

Introduction

In this work we study the out of equilibrium quantum dynamics in a XY-SPIN-1 finite chain following a protocol of quantum quench. The work done is theoretical, and to the best knowledge of the author corresponds to a previously unsolved problem.

We explain the motivation of the work, and put it into context within the relevant literature in the first section *Motivation for the work*.

The proposed work for this Thesis, and the main problems to be studied are presented in *Proposal*.

We show the methods used in the second section *Methods*. We explain the methods used to study the dynamical evolution of the system in *System evolution*; we give a short introduction to both classical and quantum information in *Concepts of Classical Information* and *Concepts of Quantum Information*; we explain the methods used to study entropy related properties in the chain in *Entropies and Correlations*.

The required resources for the development of the work are presented in *Resources*.

1.1 Motivation for the work

Quantum simulators [1, 2] open new lines of research with applications to many-body quantum systems and quantum chemistry [3]. Due to the exponential growth of the Hilbert Space in many-body systems [4, 5] an exact study of out of equillibrium dynamics becomes quickly intractable with classical computers. However, this study is experimentally possible with quantum simulators. Several experimental platforms exist, which are based on quantum superconducting circuits [6–9], trapped ions [10], trapped atoms [11] and ultra cold atoms [12, 13].

Despite the advantages offered by these quantum simulators, the study of many-body quantum systems making use of classical tools remains of interest [14]. Of special interest is the determination of universal properties shared by many-body quantum systems independently of their microscopic constituents [15]. For example, dynamical quantum phase transitions that can be characterized with suitable order parameters [16].

The XY-SPIN-1 chain model studied in this thesis, was chosen due to its similar structure to the Jaynes-Cummings Hubbard [17, 18] and Bose-Hubbard models [19]. All three models consist of a local non-linear term in each site of the lattice plus an interacting *hopping* term between sites, but their constituents are of different microscopic nature. The Jaynes-Cummings Hubbard treats with two-level atoms in cavities, the Bose-Hubbard model treats spinless bosons, whereas the proposed XY-SPIN-1 model treats spin-1 particles. Due to the difference in its microscopic components the selection of the model obeys the aforementioned search for universality in the out of equilibrium dynamics of many-body systems.

In this direction, one of the main objectives of this work is to identify an order parameter quantifying a dynamical quantum phase transition following a protocol of *quantum quench*, similar to the documented in previous works [16, 20].

A salient feature of many-body quantum systems is *entanglement* [21–24]. One of the main motivations to study entanglement in quantum systems, is that it can be used as a resource for quantum computation algorithms [24], which can not be created with Local Operations and Clasical Comunication (LOCC) [25]. Furthermore, entropies and entanglement related measurements have been used to characterize out of equilibrium dynamics and quantum phase transitions in the Bose-Hubbard model [26] and Heisenberg Spin 1/2 chains [27–32]. Therefore, the study of entropy and entanglement related quantities in spin-1 models is of interest.

A further motivation is the recent successful simulation of an Spin-1 model with single-ion anisotropy in a platform based on ultra cold atoms [33]. The model simulated in the work of Chung *et. al.*, only differs from the proposed model in an interaction term of the spin-z component of adjacent spins in the lattice. Therefore, the methods developed in this work can be used in the future to characterize the out of equilibrium dynamics of the model studied in [33].

1.2 Proposal

In this work we will study the out of equilibrium dynamics of a in general non-solvable spin-1 finite chain. The out of equilibrium dynamics will be generated following a protocol of quantum quench. In general, in a quantum quench protocol [34] the system is initialized in the ground state $|\psi_0\rangle$ of some initial Hamiltonian $H_0 \equiv H(\lambda_0)$, at a value λ_0 of some tunable parameter λ of a more general Hamiltonian $H(\lambda)$. Then at a time t, say $t = 0$, this parameter λ is suddenly change to a new value λ_f. If the initial state $|\psi_0\rangle$ is not an eigenstate of $H(\lambda_f)$ then a non-trivial out of equilibrium dynamics emerges.

The spin-1 model consider here is an specific case of the most general XXZ-spin-1 Heinsenberg chain

$$H = \sum_{\langle i,j \rangle} \left[J(\hat{S}_i^x \hat{S}_j^x + \hat{S}_i^y \hat{S}_j^y) + J_z(\hat{S}_i^z \hat{S}_j^z) \right] + p \sum_i (\hat{S}_i^z)^2. \tag{1.2.0.1}$$

The ground state of this model has been well studied in the past, and its phase diagram is now well known [35]. A recent work studied several different quench dynamics in this model with long-chains [36]. Also, the different quantum phase transitions for the case $p = 0$ have been characterized in terms of quantum discord and quantum coherence in [37].

Here, we will focus on the model with $J_z = 0$, and both the interaction between spins, and the local anisotropy are negative

$$H = -p \sum_{i=1}^{N} (\hat{S}_i^z)^2 - J \sum_{i=1}^{N-1} (\hat{S}_i^x \hat{S}_{i+1}^x + \hat{S}_i^y \hat{S}_{i+1}^y). \tag{1.2.0.2}$$

Recently the out of equilibrium dynamics of a very similar model was experimentally studied in [33]. The difference with our model appears in the value of $J_z = J$ in their model. The main observable studied in their experimental setup was the longitudinal spin alignment $A \equiv 2 - 3\langle(\hat{S}^z)^2\rangle$. To the best of our knowledge, the emerging dynamics following a quench protocol of the model we proposed has not been studied before. We will focus on the cases of lattices with $N = 2$ and $N = 3$ sites.

In our quench protocol p is a fix parameter, and J will be the tunable parameter. Therefore, our Hamiltonian H is given as a function of J, $H = H(J)$. We initially set $J_0 = 0$ and initiate the system in the eigenstate of $H(0)$ with a longitudinal spin alignment of 2. We will study the emerging dynamics of the unitary evolution that follows from the full Hamiltonian (1.2.0.2) acting on the initial state for different values of J_f. We remark that our initial state is completely classical, in the sense that any measure of quantum information on it is 0.

We first ask, is it possible to obtain with this model a maximally entangled state of two spins starting from a completely classical state? We find that it is indeed possible. We give a detailed analysis of the entanglement evolution in chapter 2 *Results*, specifically in the sub-section *Bipartite Entropies*.

In order to determine a proper dynamical order parameter, we analyze the time average of spin-z correlations. We also analyze the time average of the bipartite entropies. As we are interested in the averages taken over some time T, we ask ourselves, which is the value of T that will give us the most information about the emerging dynamics? As commented in the reference [16], we expect that the time at which finite-size effects start to dominate the dynamics will be important, and therefore we do a thorough study of the different emerging time-scales thorough the J/p spectrum. In the sub-sections *Effective Hamiltonian* and *States and observables evolution* of *Trimer* in chapter 2, we explore the origins of the different emerging time scales of the trimer. We also compare the information that both the two point spin-z correlation functions, and the bipartite entropies averages give of the different emerging dynamical regimes in the subsections *Spin-z Correlations* and *Bipartite Entropies*.

Furthermore, we will explore signatures of a dynamical-quantum phase transition (DQPT) in our finite chains. In general a DQPT is characterized by non-analicities in the rate function $\lambda(t)$ of the Loschmidt echo $\mathcal{L}(t)$ defined as $\lambda(t) \equiv -\ln(\mathcal{L}(t))/N$ in the thermodynamic limit (i.e. $N \to \infty$) [34]. In general, it is uncertain weather or not the non-analicities in the rate function will occur in a finite model if a DQPT occurs in

the thermodynamic limit, or if a DQPT will occur in the thermodynamic limit if non-analicities in the rate function appear in the finite case. For example, in a very recent study in the out of equilibrium dynamics of the 1-D transverse field Ising model, it was found that in the finite chain non-analicities in the rate functions appeared only for discrete values of the quench parameters [38]. We will explore if non-analicities appear in the evolution of the rate function of our spin-1 model, and if they appear only for discrete values of J/p or in a continuum spectrum of it. We present our results of this exploration in the subsections *States and Observables Evolution* of chapter 2.

Finally, we will also explore how the mutual information is distributed in the chain for the different emerging dynamical regimes. We will try to define the role of the parity symmetry of the system in how it is distributed. We present tentative results on this topic in the subsection *Mutual Information* of chapter 2.

In the methods section, we show the basic methods that we used to study the evolution of a many-body spin-1 system. We give a pedagogical introduction to simple fundamental concepts of both classical and quantum information theory.

1.3 Methods

1.3.1 Spin 1 Operators

Spin operators, S^α with $\alpha = x, y, z$; are Hermitian operators that satisfy the commutation relations [39]

$$\left[\hat{S}^\alpha, \hat{S}^\beta\right] = i\hbar \sum_{\gamma=x,y,z} \varepsilon_{\alpha\beta\gamma}\hat{S}^\gamma \quad \text{for any} \quad \alpha, \beta = x, y, z. \tag{1.3.1.1}$$

Where $\varepsilon_{\alpha\beta\gamma}$ is the Levi-Civita tensor which satisfies

$$\varepsilon_{\alpha\beta\gamma} = \begin{cases} 1 & \text{for even permutations of } x, y, z \\ -1 & \text{fir odd permutations of } x, y, z \\ 0 & \text{otherwise} \end{cases} \tag{1.3.1.2}$$

Spin operators act on the $(2S+1)$ Hilbert Space $\mathcal{H}_S$ and $\hat{S}^2 \equiv \hat{S}^{x^2} + \hat{S}^{y^2} + \hat{S}^{z^2} = S(S+1)\mathbb{1}$. The most common basis used is the set of eigenstates of the $\hat{S}^z$ spin-z operator, $\{|\psi^\sigma\rangle\}$, which satisfy

$$\hat{S}^z |\psi^\sigma\rangle = \sigma |\psi^\sigma\rangle, \tag{1.3.1.3}$$

$$\hat{S}^\pm |\psi^\sigma\rangle = \sqrt{S(S+1) - \sigma(\sigma \pm 1)}\, |\psi^{\sigma\pm1}\rangle \quad \text{with} \quad \hat{S}^\pm \equiv \hat{S}^x \pm i\hat{S}^y, \tag{1.3.1.4}$$

$$\langle\psi^\sigma|\psi^\sigma\rangle = 1. \tag{1.3.1.5}$$

An usual representation for the states $|\psi^\sigma\rangle$ is in column vector form; which is the representation followed in this work.

$$|\psi^\sigma\rangle = \begin{pmatrix} 0 \\ \vdots \\ 1 \\ 0 \\ \vdots \\ 0 \end{pmatrix}, \tag{1.3.1.6}$$

whose elements are all zero with exception of the element in the $S - \sigma + 1$ row which is one. For $S = 1$, using relations (1.3.1.3), (1.3.1.4) one finds the spin-1 operators in matrix form:

$$\hat{S}^x = \frac{1}{\sqrt{2}}\begin{pmatrix} 0 & 1 & 0 \\ 1 & 0 & 1 \\ 0 & 1 & 0 \end{pmatrix}, \qquad \hat{S}^y = \frac{1}{\sqrt{2}}\begin{pmatrix} 0 & -i & 0 \\ i & 0 & -i \\ 0 & i & 0 \end{pmatrix}, \qquad \hat{S}^z = \begin{pmatrix} 1 & 0 & 0 \\ 0 & 0 & 0 \\ 0 & 0 & -1 \end{pmatrix}. \tag{1.3.1.7}$$

The corresponding eigenstates, $|\psi_i^\sigma\rangle$ with $i = x, y, z$, are therefore:

$$\begin{aligned} |\psi_z^1\rangle \equiv |+1\rangle &= \begin{pmatrix} 1 \\ 0 \\ 0 \end{pmatrix}, & |\psi_z^0\rangle \equiv |0\rangle &= \begin{pmatrix} 0 \\ 1 \\ 0 \end{pmatrix}, & |\psi_z^{-1}\rangle \equiv |-1\rangle &= \begin{pmatrix} 0 \\ 0 \\ 1 \end{pmatrix}. \\ |\psi_x^1\rangle &= \frac{1}{2}\begin{pmatrix} 1 \\ \sqrt{2} \\ 1 \end{pmatrix}, & |\psi_x^0\rangle &= \frac{1}{\sqrt{2}}\begin{pmatrix} -1 \\ 0 \\ 1 \end{pmatrix}, & |\psi_x^{-1}\rangle &= \frac{1}{2}\begin{pmatrix} 1 \\ -\sqrt{2} \\ 1 \end{pmatrix}. \\ |\psi_y^1\rangle &= \frac{1}{2}\begin{pmatrix} -1 \\ -i\sqrt{2} \\ 1 \end{pmatrix}, & |\psi_y^0\rangle &= \frac{1}{\sqrt{2}}\begin{pmatrix} 1 \\ 0 \\ 1 \end{pmatrix}, & |\psi_y^{-1}\rangle &= \frac{1}{2}\begin{pmatrix} -1 \\ i\sqrt{2} \\ 1 \end{pmatrix}. \end{aligned} \tag{1.3.1.8}$$

The above are the spin-1 matrix and vector representations used in the rest of this work. Numerically they are build with the Python package NUMPY [40]; specifically as the object type numpy array.

1.3.2 Hamiltonian and States construction

1.3.2.1 Many-body states and Operators

In general, a many-body state in a spin chain with n spins of dimension d is represented as follows

$$|\psi\rangle = \sum_{i_1,i_2,\ldots i_n}^{d} c_{i_1 i_2 \ldots i_n} |i_1\rangle \otimes |i_2\rangle \cdots \otimes |i_n\rangle \equiv \sum_{i_1,i_2,\ldots i_n}^{d} c_{i_1 i_2 \ldots i_n} |i_1, i_2 \ldots i_n\rangle , \tag{1.3.2.1}$$

where $\otimes$ symbolizes a Kronecker product and the states $|i_j\rangle$ are the possible states of each spin in the chain.

An operator is local if it is defined only on one site of the chain. For example, the local spin-z operator defined in the site two of a chain with three spins would be written as

$$\hat{S}_2^z = \mathbb{1} \otimes \hat{S}^z \otimes \mathbb{1}. \tag{1.3.2.2}$$

A non-local operator is one that is defined on more that one site of the chain. For example, the spin-x interaction operator between adjacent spins one and two in a chain of three spins is written as

$$\hat{S}_1^x \hat{S}_2^x = \hat{S}^x \otimes \hat{S}^x \otimes \mathbb{1}. \tag{1.3.2.3}$$

The dimension of any operator acting on a spin-1 chain of N sites will be $3^N \times 3^N$. In general the global operators will be averaged over the number of sites in the chain, for example the $\hat{S}^z$ operator for a chain with N sites will be

$$\hat{S}^z = \frac{1}{N} \sum_{i=1}^{N} \hat{S}_i^z. \tag{1.3.2.4}$$

Numerically the many-body states and operators are build using the Python package NUMPY; specifically the built-in function kron.

1.3.2.2 Hamiltonian

The Hamiltonian studied along this thesis reads

$$H = -\hbar p \sum_{i=1}^{N} (\hat{S}_i^z)^2 - \hbar J \sum_{j=1}^{N-1} \left(\hat{S}_j^x \hat{S}_{j+1}^x + \hat{S}_j^y \hat{S}_{j+1}^y \right), \tag{1.3.2.5}$$

which can be equivalently written as

$$H = -\hbar p \sum_{i=1}^{N} (\hat{S}_i^z)^2 - \hbar J \sum_{j=1}^{N-1} \frac{1}{2} \left(\hat{S}_j^+ \hat{S}_{j+1}^- + \hat{S}_j^- \hat{S}_{j+1}^+ \right), \tag{1.3.2.6}$$

The equality follows directly from the definition of $\hat{S}_i^{\pm} \equiv \hat{S}_i^x \pm i\hat{S}_i^y$.

Numerically the Hamiltonian for any number of sites N is built using the Python package NUMPY; and specifically the built-in functions kron, and add.

1.3.2.3 Eigenstates and Eigenfrequencies

The eigenstates and eigenfrequencies are obtained numerically (and analytically when possible) by diagonalization of the Hamiltonian for the chain with 2 and 3 sites. The numerical diagonalization is calculated using the Python package NUMPY, specifically the built-in function eigh of the sub-package LINEAR ALGEBRA.

1.3.2.4 Parity operator

The parity operator Π is usually defined as the space reflection operator $\mathbf{x} \to -\mathbf{x}$ [41]. In this work the term *parity operator* refers to the spatial reflection of the chain when the origin of coordinates is set at half chain, which coincides with a bond or a particle for even and odd N respectively. For example, for $N = 2$ the parity operator over all the possible configurations in the Hilbert Space is defined as follows

$$\begin{array}{ccc} \Pi\,|+1,+1\rangle = |+1,+1\rangle\,, & \Pi\,|+1,0\rangle = |0,+1\rangle\,, & \Pi\,|+1,-1\rangle = |-1,+1\rangle\,, \\ \Pi\,|0,+1\rangle = |+1,0\rangle\,, & \Pi\,|0,0\rangle = |0,0\rangle\,, & \Pi\,|0,-1\rangle = |-1,0\rangle\,, \\ \Pi\,|-1,+1\rangle = |+1,-1\rangle\,, & \Pi\,|-1,0\rangle = |0,-1\rangle\,, & \Pi\,|-1,-1\rangle = |-1,-1\rangle\,. \end{array} \tag{1.3.2.7}$$

Therefore, the matrix form of the parity operator for $N = 2$ spin-1 particles in the z-basis simply reads

$$\begin{pmatrix} 1 & 0 & 0 & 0 & 0 & 0 & 0 & 0 & 0 \\ 0 & 0 & 0 & 1 & 0 & 0 & 0 & 0 & 0 \\ 0 & 0 & 0 & 0 & 0 & 0 & 1 & 0 & 0 \\ 0 & 1 & 0 & 0 & 0 & 0 & 0 & 0 & 0 \\ 0 & 0 & 0 & 0 & 1 & 0 & 0 & 0 & 0 \\ 0 & 0 & 0 & 0 & 0 & 0 & 0 & 1 & 0 \\ 0 & 0 & 1 & 0 & 0 & 0 & 0 & 0 & 0 \\ 0 & 0 & 0 & 0 & 0 & 1 & 0 & 0 & 0 \\ 0 & 0 & 0 & 0 & 0 & 0 & 0 & 0 & 1 \end{pmatrix}. \tag{1.3.2.8}$$

This is clearly a SWAP gate between the sites 1 and 2 of the chain. In general, by writing the SWAP gate between sites i and j of the chain as Π^i_j, the parity operator reads

$$\Pi = \begin{cases} \sum_{i=0}^{(N-2)/2} \Pi^{i+1}_{N-i} & \text{for } N \text{ even}, \\ \sum_{i=0}^{(N-3)/2} \Pi^{i+1}_{N-i} & \text{for } N \text{ odd}. \end{cases} \tag{1.3.2.9}$$

The parity operator Π is such that the square of it is the identity $\Pi^2 = \mathbb{1}$. Therefore, its unique eigenvalues are ± 1.

The parity operator, for any general N, is build with an user defined function in Python, using the packages NUMPY and ITERTOOLS [42].

1.3.3 System evolution

1.3.3.1 Unitary Evolution

The dynamics of the system is given by the Schrödinger equation

$$i\hbar \frac{\partial\,|\psi(t)\rangle}{\partial t} = H\,|\psi(t)\rangle\,, \tag{1.3.3.1}$$

which will be solved numerically and analytically for the two particle case. For the numerical solutions the evolution operator will be used

$$\mathcal{U}(t) = \exp(-iHt/\hbar) = \exp(-iHtp), \tag{1.3.3.2}$$

where the second equality holds as $\hbar = 1$ throughout this work, and p can be factored out of the Hamiltonian (1.3.2.5)

$$H = p\left(-\sum_{i=1}^{N}(\hat{S}^z_i)^2 - \frac{J}{p}\sum_{i=1}^{N-1}\hat{S}^x_i\hat{S}^x_{i+1} + \hat{S}^y_i\hat{S}^y_{i+1}\right). \tag{1.3.3.3}$$

We are also setting $p = 1$, and therefore the time t will be in units of p^{-1}.

The state of the system at time t for a given initial state will be

$$|\psi(t)\rangle = \mathcal{U}(t)\,|\psi(0)\rangle\,. \tag{1.3.3.4}$$

The matrix exponential of the Hamiltonian will be numerically calculated using the Python package SCIPY; specifically the built-in function expm.

Another option is to build the evolution operator for a small Δt and apply it consecutively to the initial state. The first steps of this iteration are here illustrated

$$|\psi(\Delta t)\rangle = \mathcal{U}(\Delta t)\,|\psi(0)\rangle \to |\psi(2\Delta t)\rangle = \mathcal{U}(\Delta t)\,|\psi(\Delta t)\rangle \to |\psi(3\Delta t)\rangle = \mathcal{U}(\Delta t)^3\,|\psi(0)\rangle\,, \tag{1.3.3.5}$$

and in general

$$|\psi(n\Delta t)\rangle = \mathcal{U}(\Delta t)^n\,|\psi(0)\rangle\,, \tag{1.3.3.6}$$

In this way the exponential of a matrix has to be calculated only once, and not at each value of t. Therefore, the algorithm for calculating the evolution is more efficient.

It was checked that the error given by this second method with $\Delta t = 10^{-4}$ was for all purposes negligible. See figure 1.1 for a comparison between the states given by the two methods, for lattice number of sites $N = 3$ with the initial state $|\psi_0\rangle \equiv |0, 0, 0\rangle$ and a ratio of $J/p = 10$.

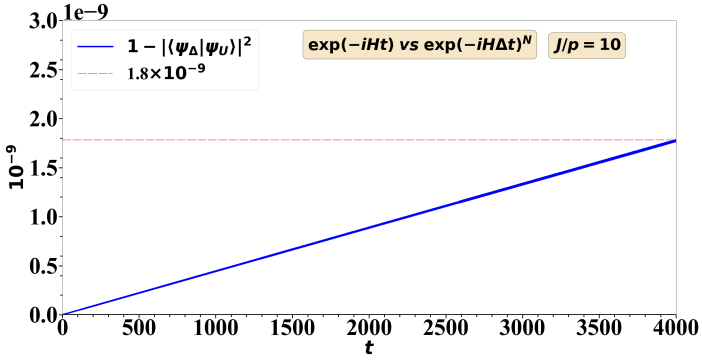

Figure 1.1: Comparison between $|\psi(t)_U\rangle$ calculated via the exact unitary operator at each value of t versus $|\psi(t)_\Delta\rangle$ calculated with successive applications of the unitary operator for a small $\Delta t = 10^{-4}$. The time axis is given in units of p^{-1}. The difference grows linearly with time and for all physical purposes is negligible within the simulating time.

1.3.3.2 Averages of relevant quantities

In this work, several quantities of interest will be averaged over a time interval T. Let $C(t)$ be any observable or function of interest calculated from the wavefunction $|\psi(t)\rangle$ at any specific t; the time average $\overline{C(t)}$, is defined as

$$\overline{C(t)} = \frac{1}{T}\int_0^T C(t)dt. \tag{1.3.3.7}$$

Numerically, this is calculated with a time step $\Delta t = 10^{-3}$ between points of $C(t)$. $C(t)$ is calculated and saved for $t = 0.000, 0.001, 0.002\ldots$ and so on. The integral is calculated using the built in function of the SCIPY [43] package integrate.simps, which uses the Simpson rule to evaluate it.

1.3.3.3 Expectation value of observables

The expectation value of any observable $\hat{O}$ in the state $|\psi(t)\rangle$, is given by

$$\langle \hat{O} \rangle = \langle \psi(t) | \hat{O} | \psi(t) \rangle \,. \tag{1.3.3.8}$$

Alternatively by using the density matrix $\rho(t) \equiv \rho(|\psi(t)\rangle) = |\psi\rangle\langle\psi|$ the expectation value reads

$$\langle \hat{O} \rangle = \mathrm{tr}\Big(\hat{O}\rho\Big). \tag{1.3.3.9}$$

In this work expectation values are numerically calculated using equation (1.3.3.8). This is preferred because we are studying a closed system and storing the density matrices $\rho(t)$ uses exponentially more memory than storing the states $|\psi(t)\rangle$ in vector form.

The matrix multiplications and inner products are performed using the Python package NUMPY; specifically the built-in functions `matmul` or `dot`.

1.3.4 Concepts of Classical Information Theory

1.3.4.1 Shannon Entropy

Information theory was initiated by Shannon's seminal paper *A Mathematical Theory of Communication* [44]. One of the key questions posed in it was: *in a given discrete information source, at what rate information is produced in it?*; which lead him to the correlated question, *can we find a measure of how uncertain we are of the outcome of an specific event?*.

Before laying out the answer given by Shannon to the second question, some simple definitions are suited. An event, Ω, can be understood as a physical process that may have discrete (like a coin toss) or continuous (like the momentum of a particle) outcomes and has a probability distribution associated with it. A random variable X is a mapping from an event Ω to a probability distribution associated with its possible outcomes; therefore, from the point of view of classical information theory the specific properties of the physical system are non-relevant, being the random variable associated with it what it is studied. Suppose the possible outcomes of an event Ω are continuous. In that case, the random variable X associated with it will also be continuous and will map the outcomes to a continuous probability distribution (this would be the typical $|\psi|^2$ of the wavefunction describing the probability density of a particle); if the possible outcomes of an event Ω are discrete, then the random variable X associated to it will also be discrete, and maps the outcomes to a discrete set of probabilities $\{p(x_1), p(x_2), \dots p(x_d)\}$ where d is the total number of possible outcomes (for the spin-1 value of a particle in a specific direction d would be equal to three). For a more complete and formal definition of a random variable see chapter one of Ref. [45]. In this work and in the following discussion, we only considered discrete sample space of events.

In its work, Shannon proceeded with an axiomatic approach, stating the properties that a function that measures the amount of uncertainty of a given event should have. The interested reader is compelled to see the original publication [44] for the details of this derivation, which lead him to define what is known as the Shannon Entropy.

For a random variable $X(p(x_1), p(x_2), \dots p(x_d))$ its Shannon entropy, $H(X)$, is defined as:

$$H(X) = H(p(x_1), p(x_2), \dots p(x_d)) = -\sum_{i=1}^{d} p_i \log_2 p_i, \tag{1.3.4.1}$$

with $0 \log_2 0 \equiv 0$. In general, for a random variable X with d possible outcomes the maximum entropy is $\log_2 d$.

Therefore, the Shannon entropy it is understood as the *uncertainty* that an observer has on the outcome of an event or about the state of a system *before* it is measured. Or reciprocally, it can be understood as the *amount* of information *gained* when a measurement is performed in the system or the outcome of the event is known [24].

For more details about the meaning and motivation of the Shannon Entropy, the interested reader is recommended to see [24, 44, 46].

1.3.4.2 Joint Entropy and Conditional Entropy

In classical information theory the *joint entropy*, $H(X,Y)$, of two random variables X and Y is defined as

$$H(X,Y) = -\sum_{x\in X, y\in Y} p(x,y)\log_2 p(x,y), \tag{1.3.4.2}$$

where $p(x,y)$ is the probability of both events x and y to occur. The join entropy it is interpreted as the uncertainty of the joint probability distribution of X and Y before it's measured.

The *conditional entropy*, $H(Y|X)$, for two random variables X and Y is defined as

$$H(Y|X) = -\sum_{x\in X, y\in Y} p(x,y)\log_2 p(y|x), \tag{1.3.4.3}$$

where $p(y|x)$ means the probability of event y given that event x occurred. It is worthwhile giving some concrete examples to illustrate its meaning.

In the toss of two coins which are represented by random variables $X(p(h_1), p(t_1))$ and $Y(p(h_2), p(t_2))$, where $p(h_1)$ and $p(t_1)$ respectively are the probability of the first coin to fall on heads or tails, and $p(h_2)$ and $p(t_2)$ respectively are the probability of the second coin to fall on heads or tails. If the toss is assumed to be fair, that is the probability of heads and tails is the same for both coins, the joint entropy is given by

$$\begin{aligned} H(X,Y) &= -p(h_1,h_2)\log_2 p(h_1,h_2) - p(h_1,t_2)\log_2 p(h_1,t_2) - p(t_1,h_2)\log_2 p(t_1,h_2) - p(t_1,t_2)\log_2 p(t_1,t_2) \\ &= -4\times\left(\frac{1}{4}\log\frac{1}{4}\right) = \log_2 4 = 2. \end{aligned} \tag{1.3.4.4}$$

And the conditional entropy $H(Y|X)$ is given as

$$\begin{aligned} H(Y|X) &= -p(h_1,h_2)\log_2 p(h_2|h_1) - p(h_1,t_2)\log_2 p(t_2|h_1) - p(t_1,h_2)\log_2 p(h_2|t_1) - p(t_1,t_2)\log_2 p(t_2|t_1) \\ &= -4\times\left(\frac{1}{4}\log_2\frac{1}{2}\right) = \log_2 2 = 1; \end{aligned} \tag{1.3.4.5}$$

which is the entropy of $H(Y)$, and therefore the random variables X and Y are completely uncorrelated, which is equivalent to say that no information about the state of the second coin is gained when we know the state of the first one.

On the other hand, take for example the electric circuit formed by a switch which can have values open or closed, connected to a battery and a led light which can be either on or off, and will always be on if the switch is closed (or off if the switch is open).

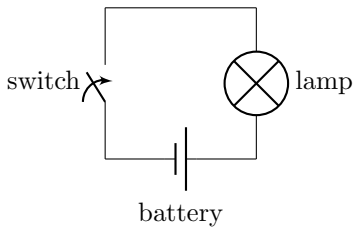

The switch and the light are represented by random variables $X(p(s_o), p(s_c))$ and $Y(p(l_1), p(l_0))$, where $p(s_o)$ and $p(s_c)$ respectively are the probability of the switch being open and closed, and $p(l_0)$ and $p(l_1)$ respectively

are the probability of the light being off or on. Assuming an idealized situation where all the circuit elements work perfectly, and $p(s_o) = p(s_c) = 1/2$; the joint entropy will be given by

$$\begin{aligned} H(X,Y) &= -p(s_o,l_0)\log_2 p(s_o,l_0) - p(s_o,l_1)\log_2 p(s_o,l_1) - p(s_c,l_0)\log_2 p(s_c,l_0) - p(s_c,l_1)\log_2 p(s_c,l_1) \\ &= -\frac{1}{2}\log\frac{1}{2} - 0\log 0 - 0\log 0 - \frac{1}{2}\log\frac{1}{2} = \log 2. \end{aligned} \tag{1.3.4.6}$$

The conditional entropy $H(Y|X)$ will be

$$\begin{aligned} H(Y|X) &= -p(s_o,l_0)\log_2 p(l_0|s_o) - p(s_o,l_1)\log_2 p(l_1|s_o) - p(s_c,l_0)\log_2 p(l_0|s_c) - p(s_c,l_1)\log_2 p(l_1|s_c) \\ &= -\frac{1}{2}\log_2 1 - 0\log_2 0 - 0\log_2 0 - \frac{1}{2}\log_2 1 = 0; \end{aligned} \tag{1.3.4.7}$$

therefore, the random variables X and Y are said to be completely correlated. This means that there is cero uncertainty about the outcome of Y when the outcome of X is known, or equivalently, there is zero information gained when the outcome of Y is known if the outcome of X was previously known.

An important theorem (related to mutual information) is the *chain rule* for the Shannon entropy, joint entropy and conditional entropy of two random variables X and Y; which states that

$$H(X,Y) = H(X) + H(Y|X) = H(Y) + H(X|Y). \tag{1.3.4.8}$$

This implies that

$$H(Y|X) - H(X|Y) = H(Y) - H(X); \tag{1.3.4.9}$$

thus conditional entropy is not reciprocal $H(Y|X) \neq H(X|Y)$, unless $H(X) = H(Y)$.

For proofs, interesting theorems and more results the reader is referred to [46].

1.3.4.3 Mutual Information

The mutual information, $I(x,y)$, between two random variables X and Y is defined as

$$I(X;Y) = \sum_{x,y} p(x,y)\log_2\frac{p(x,y)}{p(x)p(y)}, \tag{1.3.4.10}$$

with $0\log_2(0/0) \equiv 0$ [46].

It can be rewritten in the following form

$$I(X;Y) = H(X) - H(X|Y) = H(Y) - H(Y|X); \tag{1.3.4.11}$$

and is therefore understood as the amount of *uncertainty loss* in the random variable X when Y is known or vice versa.

Using the chain rule mutual information can equivalently be written as

$$I(X;Y) = H(X) + H(Y) - H(X,Y), \tag{1.3.4.12}$$

and is therefore also understood as the amount of information that the two random variables X and Y share.

These equalities can be summarized in the following Venn diagram:

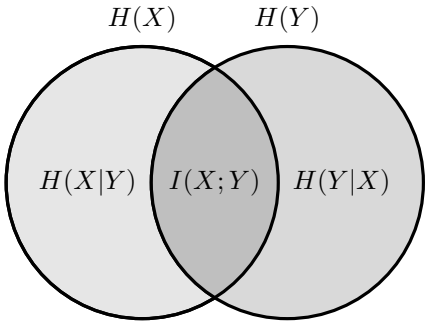

Figure 1.2: Venn diagram summarizing the classical information theory relations between the Shannon entropy, joint entropy, conditional entropy and mutual information of two random variables X and Y.

Thinking of mutual information, joint entropies and conditional entropies relations with the above diagram is always valid when treating classical random variables, but this will not be the case in quantum mechanics. This will be further discussed below in *Concepts of Quantum Information Theory*.

For proofs, interesting theorems and more results the reader is recommended to see [46].

1.3.5 Concepts of Quantum Information Theory

The Classical Information Theory concepts defined above have their corresponding analogous quantities in Quantum Information Theory, which are in principle obtained by replacing the Shannon Entropy with the von Neumann Entropy but with important subtleties added.

1.3.5.1 Von Neumann Entropy

The Von Neumann entropy of a density matrix ρ, is defined as

$$S(\rho) = -\operatorname{tr}(\rho \log \rho) = -\sum_i \lambda_i \log \lambda_i, \tag{1.3.5.1}$$

where the λ_i are the eigenvalues of ρ. Historically, Von Neumann proposed its entropy definition as a generalization to quantum mechanics of the Gibbs Entropy for a classical macroscopic state [47].

The Von Neumann entropy can also be seen as the quantum information analog of the Shannon Entropy [24, 44, 46]. Notice that the eigenstates of the density matrix in the Von Neumann entropy are analogous to the probabilities of the random variable X in the Shannon entropy. Therefore, the Von Neumann entropy can be seen as a measure of how *uncertain* we are of the state of the system before it's measured.

Further, for a pure bipartite state of two interacting quantum systems, the Von Neumann entropy is the **unique measurement of entanglement** between them [25, 48].

The reader is compelled to notice how surprising is the connection between statistical physics, information theory and entanglement theory in very similar *entropy* functions. From one end, in statistical physics Von Neumann entropy emerges as a quantum generalization of the Gibbs entropy that characterizes the *uncertainty* of a macroscopic state and is maximized in equilibrium; from the other end, in information theory emerges as the uncertainty of the information generated in a discrete information channel [44]; *and* is the unique measurement of entanglement in pure bipartite states when entanglement is understood as a quantum resource that can not be created with LOCC (Local Operations and Classical Communication) operations [25]. That all these three functions are practically the same is remarkable.

The numerical calculation of the von neumann entropy is performed with the Python package NUMPY; in specific with the built-in functions `trace`, `eigh`,`log`, and `add`.

1.3.5.2 Joint Entropy

The *joint entropy* of two subsystems A and B described by the density matrix ρ_{AB}, is defined as [24]

$$S(A,B) = S(\rho_{AB}) = -\operatorname{tr}(\rho_{AB}\log\rho_{AB}) = -\sum_i \lambda_i \log\lambda_i, \tag{1.3.5.2}$$

where the λ_i are the eigenvalues of ρ_{AB}. Notice that for a pure bipartite state $|\psi_{AB}\rangle$ the joint entropy is

$$S(|\psi_{AB}\rangle) = -\operatorname{tr}(\rho_{AB}\log\rho_{AB}) = 0 \quad \text{with} \quad \rho_{AB} \equiv |\psi_{AB}\rangle\langle\psi_{AB}|\,, \tag{1.3.5.3}$$

which quantifies the fact that one knows exactly the global state of the system and there is zero uncertainty about it.

A fundamental difference with its classical information analog is that it is no longer true that local uncertainties are less or equal to global uncertainties. In classical information theory is stated that

$$H(X) \leq H(Y) \leq H(X,Y) \leq H(X) + H(Y). \tag{1.3.5.4}$$

This means that the uncertainty on the random variables X and Y is *equal or less* than the global uncertainty of the joint system (X,Y), which is never greater than the sum of the entropies of X and Y independently. Therefore, if an observer has zero uncertainty about the global state of a classical system, then it will have zero uncertainty about the local state of its constituents. In quantum mechanics, this is not the case, take for example an EPR state

$$|\psi\rangle = \frac{|00\rangle + |11\rangle}{\sqrt{2}},$$

which is formed by two qubits, lets' call them the left and right qubits. Then, the global uncertainty about the state of the system formed by the two qubits is its joint entropy which is zero. The local entropies are defined for the reduced density matrix of each subsystem as

$$S(\rho_L) = -\operatorname{tr}_L(\rho_L\log\rho_L) = -\sum_i \lambda_i^L \log\lambda_i^L; \tag{1.3.5.5}$$

where the λ_i^L are the eigenvalues of the reduced density matrix ρ_L, which is defined as $\rho_L \equiv \operatorname{tr}_R(\rho)$, and indices L and R stand for left and right. The local entropies of our EPR state are

$$S(\rho_L) = S(\rho_R) = -\frac{1}{2}\log\frac{1}{2} - \frac{1}{2}\log\frac{1}{2} = \log 2; \tag{1.3.5.6}$$

and therefore $S(\rho_L) > S(\rho)$. This means that despite that an observer has zero uncertainty about the global state of the system, it has a non-zero uncertainty about the local state of its constituents.

For a pure bipartite state of two subsystems A and B, described by the density matrix ρ_{AB} it is always true that

$$S(\rho_{AB}) \leq S(\rho_A) = S(\rho_B); \tag{1.3.5.7}$$

where ρ_A and ρ_B are the reduced density matrices for subsystems A and B. The inequality and the equality follow directly from the Schmidt's decomposition of a pure bipartite state (see *Entropies and Correlations* below).

The joint entropy will be important for the definition of mutual information, and therefore for the interpretation of bipartite entropies and the definition of quantum discord.

1.3.5.3 Conditional Entropy

One of the main differences between quantum and classical information theory resides in the definition of the conditional entropy $S(A|B)$ for two subsystems A and B, which is defined in [24] as

$$S(A|B) \equiv S(A,B) - S(B), \tag{1.3.5.8}$$

a mathematical definition that allows the chain rule for classical information to still hold

$$S(A,B) = S(B) + S(A|B). \tag{1.3.5.9}$$

However, this is just a consequence of the definition and does not seem to carry any relevant physical information. Notice that defined in this way the conditional entropy may even take negative values, and if it is hoped to be interpreted as the uncertainty remaining on the state of subsytem A after the state of subsytem B is known it does not seem to be an appropriate measure.

When trying to define the conditional entropy as a function measuring the uncertainty on the state of subsystem A when the state of the subsystem B is known, we should notice that it is not a well defined quantity until a specific set of measurement operators on subsystem B is chosen [49]. For this reason, one writes the conditional entropy subject to an specific selection of measurement operators on subsytem B $\{\Pi_B\}$.

The state of the system AB described by the density matrix ρ_{AB}, after an specific measurement is done, and the outcome corresponding to Π_B^j has been detected is

$$\rho_{AB|(\Pi_B^j)} = \frac{\Pi_B^j \rho_{AB} \Pi_B^j}{\mathrm{tr}\left(\Pi_B^j \rho_{AB} \Pi_B^j\right)}. \tag{1.3.5.10}$$

Therefore, the conditional entropy for an specific set $\{\Pi_B\}$ was defined by the authors in [49] as

$$S(A|B(\{\Pi_B\})) = \sum_j p_j S(A|\Pi_B^j); \tag{1.3.5.11}$$

where p_j is the probability of obtaining the outcome associated with the projector Π_B^j. Notice that this definition does carry physical significance, and can be interpreted as the average uncertainty that an observer has on the state of subsytem A when a specific projective measurement is performed on the system B and its state is completely known.

A consequence of the difference between the classical and quantum definitions of the conditional entropy, or more precisely between the local accessible information, is that the chain rule equality in the most general case is broken. In fact it turns out to be always true that

$$S(A,B) \leq S(B) + S(A|B\{\Pi_B\}). \tag{1.3.5.12}$$

Let us call this inequality the *chain rule inequality*. Proofs of it can be found at [49] or at [50].

For pure bipartite states the conditional entropy $S(A|B\{\Pi_B\}) = S(B|A\{\Pi_A\}) = 0$. This follows from the fact that after a projective measurement on a pure state is done and an specific outcome is detected, the resulting state is also a pure state, and therefore its entropy is zero.

1.3.5.4 Mutual Information and locally accessible mutual information

The classical mutual information between two random variables X and Y, $I(X;Y)$, is defined as

$$I(X;Y) = H(X) - H(X|Y) = H(Y) - H(Y|X); \tag{1.3.5.13}$$

which means the amount of information that is gained about X when Y is known or viceversa. Using Bayes theorem it is mathematically equivalent to

$$I(X;Y) = H(X) + H(Y) - H(X,Y); \tag{1.3.5.14}$$

and is therefore also equal to the difference between the sum of the local uncertainties and the total uncertainty on the two variables system.

Following the classical definition of mutual information, the *locally accessible mutual information* between two quantum systems A and B, $J(A,B)$, can be defined as the uncertainty left in subsystem A when the state of sub-system B is known [51]

$$J(A, B\{\Pi_B\}) = S(A) - S(A|B\{\Pi_B\}); \tag{1.3.5.15}$$

which in general will not be symmetric under the exchange of A with B, as it involves an specific set of measurement projectors and in general the conditional entropy will be different for different sets.

The other possible definition for quantum mutual information between two subsytems A and B whose state is describe by the density matrix ρ_{AB}, $I(A:B)$, is the difference between the sum of local entropies with the global entropy pre-measurement

$$I(A:B) = S(A) + S(B) - S(A,B); \tag{1.3.5.16}$$

where $S(A)$ is the von neumann entropy of the reduced density matrix ρ_A. $I(A:B)$ will be simply called *mutual information*.

From the chain rule inequality it follows that

$$I(A:B) - J(A, B\{\Pi_B\}) = S(B) + S(A|B\{\Pi_B\}) - S(A,B) \geq 0. \tag{1.3.5.17}$$

This inequality will naturally lead to the definition of quantum discord as a measurement of quantum correlations as it quantifies one of the fundamental differences between classical and quantum correlations. In the former, all the shared information between two variables can be locally accessed, whereas, in the second this is in general not true. Further comments are made in *Quantum Discord* below.

1.3.6 Entropies and Correlations

1.3.6.1 Schmidt Decomposition and Purifications

A quantum system whose state $|\psi\rangle$ is known exactly is said to be in a *pure state* [24]; and it's density matrix is simply

$$\rho = |\psi\rangle\langle\psi| . \tag{1.3.6.1}$$

Otherwise, the system is said to be in a *mixed state*. A mixed state density matrix is a linear combination of the different pure states in the ensemble; and is written as

$$\rho = \sum_i p_i \, |\psi_i\rangle\langle\psi_i| . \tag{1.3.6.2}$$

The **Schmidt's decomposition** of a pure bipartite state of subsystems A and B of dimensions n and m respectively, $|\psi_{AB}\rangle$, is the following:

$$|\psi_{AB}\rangle = \sum_i^d \sqrt{\lambda_i} \, |i_A\rangle \otimes |i_B\rangle , \tag{1.3.6.3}$$

where the vectors in the sets $\{|1_A\rangle, |2_A\rangle \ldots |d_A\rangle\}$ and $\{|1_B\rangle, |2_B\rangle \ldots |d_B\rangle\}$ form an orthonormal basis of dimension d; and the λ_i are positive real coefficients. The proof of why such a decomposition exists is based on the singular value decomposition of a matrix and is given with details in [24].

The λ_i are called the *Schmidt's coefficients*; d is called the *Schmidt's number*; and the orthonormal set of vectors $\{|i_A\rangle\}, \{|i_B\rangle\}$ are called the *Schmidt's vectors*.

The Schmidt's coefficients for a pure bipartite state are unique. This is a consecuence of the fact that a pure bipartite density matrix has, by definition, an unique state which generates it; which implies that the reduced density matrix of any of the subsystems ρ_A or ρ_B is also unique. Therefore, as for a given Schmidt decomposition of a state the reduced density matrix of system A, ρ_A, is given by

$$\rho_A = \mathrm{tr}_B(\sum_{i,j} \sqrt{\lambda_i \lambda_j}\, |i_A\rangle\langle j_A| \otimes |i_B\rangle\langle j_B|) = \sum_{l=1}^{m} \sqrt{\lambda_i \lambda_j}\, |i_A\rangle\langle j_A| \otimes \langle l_B|i_B\rangle \langle j_B|l_B\rangle = \sum_{l=1}^{d} \lambda_l\, |l_A\rangle\langle l_A|\,, \quad (1.3.6.4)$$

the Schmidt's coefficients must also be unique. Notice that this is not the case for the Schmidt's vectors if one of the Schmidt's coefficients is degenerate, that is the same number appears more than once in the decomposition. In order to clarify the above statement take an EPR or Bell state

$$(|00\rangle + |11\rangle)/\sqrt{2},$$

and notice that it is already in it's Schmidt's decomposition. Also take the following state

$$(|{+}{+}\rangle + |{-}{-}\rangle)/\sqrt{2}, \quad \text{with} \quad |\pm\rangle \equiv |(0\rangle \pm |1\rangle)/\sqrt{2}.$$

It is direct to check that both states above are representations of the same state. The Schmidt's coefficients remain the same, but the Schmidt's vectors change. In general, for any degenerate Schmidt value, λ_i, any set of orthonormal vectors build as linear combinations of the Schmidt's vectors associated to the degenerate value, λ_i, will also be a set of valid Schmidt's vectors associated to it. When there are no degenerate Schmidt's values, the set of Schmidt's vectors is also unique.

The uniqueness of the Schmidt's values will be important for the Bipartite Entropies of pure states.

1.3.6.2 Bipartite Entropies

In this work, bipartite entropies are studied in the emerging dynamics of both the dimer and trimer. Their dynamical evolution and averages over relevant times are determined.

Bipartite entropies are defined for any bipartite quantum system AB, described by a density matrix ρ_{AB}, as the Von Neumann entropies of the reduced density matrices $\rho_A \equiv \mathrm{tr}_B(\rho_{AB})$ and $\rho_B \equiv \mathrm{tr}_A(\rho_{AB})$. The bipartite entropy of A is $S(A) \equiv S(\rho_A)$.

For pure bipartite states the bipartite entropy is unique and is the same for both subsystems A and B. This follows from writing the state in its Schmidt's decomposition

$$|\psi\rangle = \sum_i \sqrt{\lambda_i}\, |i_A\rangle \otimes |i_B\rangle \to \rho_A = \sum_i \lambda_i\, |i_A\rangle\langle i_A|\,, \qquad \rho_B = \sum_i \lambda_i\, |i_B\rangle\langle i_B| \implies S(A) = S(B). \quad (1.3.6.5)$$

For a general pure state of a many-body system, $|\psi\rangle$, bipartite entropies are defined for specific *bipartitions* of it. It is always possible to write any pure many-body system state as a pure bipartite state with an specific bipartition. To show this, first notice that any product state of a quantum many-body system with n sub-systems, each of them of dimension m_i which can be written as

$$\left|e_{\{j_k\}}\right\rangle = |j_1\rangle \otimes |j_2\rangle \otimes \cdots \otimes |j_m\rangle\,, \text{where } \{j_k\} \text{ represents the set } \{j_1, j_2, \ldots j_n\},$$

can be mathematically decomposed in two sub-systems A and B.

For example, let $n = 3$ and $m_1 = m_2 = m_3 = 3$; then all product states can be written as

$$\left|e_{\{j_k\}}\right\rangle = |j_1\rangle \otimes |j_2\rangle \otimes |j_3\rangle\,, \quad \text{with} \quad j_i = 1, 2, 3. \quad (1.3.6.6)$$

The set of all different possible bipartitions, $A - B$, is $\{12-3, 13-2, 1-23\}$. The bipartition $12-3$ means that one is taking A as the system formed by the sub-systems 1 and 2, and B as the system formed by sub-system 3. See figure 1.3.

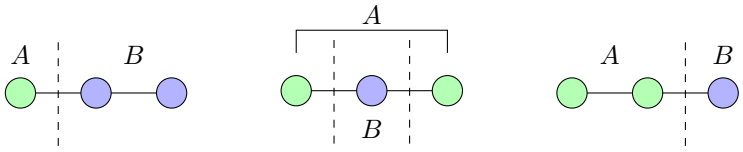

Figure 1.3: Possible bipartitions of a three particle system. From left to right $1-23, 13-2, 12-3$.

A basis set for A is the one formed by the states

$$\left|A_{\{j_k\}}\right\rangle = |j_1\rangle \otimes |j_2\rangle\,, \quad \text{with} \quad j_1, j_2 = 1, 2, 3; \tag{1.3.6.7}$$

which can be reshaped as

$$|A_l\rangle = |j_1, j_2\rangle_l = |j_1\rangle \otimes |j_2\rangle \quad \text{with} \quad 1 \leq l \leq 9,\ l \in \mathbb{N}, \tag{1.3.6.8}$$

with a simple mapping $(j_1, j_2) \to l$ ($(1,1) \to 1; (1,2) \to 2$ and so on). A basis set for B is defined in the same way

$$|B_k\rangle = |j_3\rangle\,, \quad \text{with} \quad j_3 = 1, 2, 3; \tag{1.3.6.9}$$

without the need of reshaping and mapping as B is formed by only one subsystem. Then, in this new basis the product state $\left|e_{\{j_k\}}\right\rangle$ can be rewritten as

$$\left|e_{\{j_k\}}\right\rangle = |A_l\rangle \otimes |B_k\rangle\,, \tag{1.3.6.10}$$

and therefore it is mathematically equivalent to a pure bipartite state of systems A and B, with dimensions $3 \times 3 = 9$ and 3 respectively.

Now take a general quantum system of N sub-systems, where each sub-system i has dimension m_i and basis $\{|i_1\rangle, |i_2\rangle, \ldots, |i_{m_i}\rangle\}$. A complete set of basis states for the system is formed by the set of all $\left|e_{\{j_i\}}\right\rangle$ product states as defined above. As any state can be written as a linear combination of product states

$$|\psi\rangle = \sum_{\{j_i\}} c_{\{j_i\}} \left|e_{\{j_i\}}\right\rangle, \tag{1.3.6.11}$$

it follows that it can be rewritten as a pure bipartite state

$$|\psi\rangle = \sum_{\{j_i\}} c_{\{j_i\}} |A_{j_A}\rangle \otimes |B_{j_B}\rangle\,; \tag{1.3.6.12}$$

and therefore it can be written in its Schmidt decomposition by using its singular value decomposition. In this way the bipartite entropy is uniquely defined for any pure bipartite state independent from the dimensions of its sub-systems.

For pure bipartite states the bipartite entropy is half the mutual information

$$I(A:B) = S(A) + S(B) - S(A,B) = 2S(A) = 2S(B); \tag{1.3.6.13}$$

as $S(A,B) = 0$ because it is a pure state. It is also exactly equal to the locally accessible mutual information

$$J(A, B\{\Pi_B\}) = J(B, A\{\Pi_A\}) = S(A) - S(B|A\{\Pi_A\}) = S(B) - S(A|B\{\Pi_B\}) = S(A) = S(B). \tag{1.3.6.14}$$

as $S(B|A\{\Pi_A\}) = S(A|B\{\Pi_B\}) = 0$ for pure states as explained above at the end of *conditional entropy*.

In the literature bipartite entropies are sometimes referred as *entanglement entropies* [32, 52, 53]. It has been found that they signal quantum phase transitions in spin-chains, both static and dynamical [15, 26, 32, 54].

Numerically, bipartite entropies were calculated with an user defined function in Python using the library NUMPY; specifically with the functions kron, matmul, log, eigh.

1.3.6.3 Quantum Discord

During the development of this work the Quantum Discord evolution and averages over relevant times were studied in the trimer emerging dynamics, but the results and analysis are left to be presented elsewhere.

In classical information theory two identical measurements of mutual information are $I(A,B)$ and $J(A,B)$

$$I(A;B) = H(A) + H(B) - H(A,B), \tag{1.3.6.15}$$
$$J(A,B) = H(A) - H(A|B) = H(B) - H(B|A), \tag{1.3.6.16}$$

which can be shown to be equal using the classical information chain rule. When these measurements are generalized to quantum systems one gets the *mutual information* $I(A:B)$

$$I(A:B) = S(A) + S(B) - S(A,B), \tag{1.3.6.17}$$

and the *locally accessible mutual information* $J(A,B\{\Pi_B\})$

$$J(A,B\{\Pi_B\}) = S(A) - S(A|B\{\Pi_B\}); \tag{1.3.6.18}$$

as explained above in *concepts of classical information theory* and *concepts of quantum information theory.*

Quantum discord was originally defined in the work of Ollivier and Zurek [49] as the difference between the *mutual information* $I(A,B)$ and the *locally accessible mutual information* $J(A,B\{\Pi_B\})$

$$\begin{aligned}\delta(A,B\{\Pi_B\}) &= I(A:B) - J(A,B\{\Pi_B\}) \\ &= S(B) + S(A|B\{\Pi_B\}) - S(A,B).\end{aligned} \tag{1.3.6.19}$$

Notice therefore that quantum discord is a measurement of how broken is the *mutual information chain rule* for quantum systems for some set $\{\Pi_B\}$ of projective local measurements.

At a similar time Henderson and Vedral [55] proposed a measurement for the classical correlations in a bipartite quantum system $Q(A,B)$. The proposed measurement was the maximal value of the *locally accessible mutual information*:

$$Q(A,B) = \sup_{\{\Pi_B\}} J(A,B\{\Pi_B\}) = S(A) - \min_{\{\Pi_B\}} S(A|B\{\Pi_B\}); \tag{1.3.6.20}$$

where it is not in general true that $\sup_{\{\Pi_B\}} J(A,B\{\Pi_B\}) = \sup_{\{\Pi_A\}} J(B,A\{\Pi_A\})$ [56]. This leads to the more physically relevant definition of quantum discord as

$$\delta(A,B) = I(A:B) - Q(A,B) = S(B) + \min_{\{\Pi_B\}} S(A|B\{\Pi_B\}) - S(A,B); \tag{1.3.6.21}$$

which is interpreted as the amount of *quantum correlations* between systems A and B. Discord is in general not symmetrical under the change $A \to B \implies \delta(A,B) \neq \delta(B,A)$.

Note that for a pure bipartite state the quantum discord is exactly equal to the bipartite entropy

$$\delta(A,B) = S(B) - S(A,B) + \min S(A|B\{\Pi_B\}) = S(B) = S(A); \tag{1.3.6.22}$$

due to the fact that for a pure bipartite state $S(A,B) = 0$, $S(A|B\{\Pi_B\}) = S(B|A\{\Pi_A\}) = 0$ and $S(A) = S(B)$ as explained above in *Bipartite Entropies* and *Conditonal Entropy.*

Quantum discord has been found to identify critical points in quantum phase transitions [29, 37, 57, 58]. It has further interests in several areas, including quantum algorithms, quantum information, thermodynamics [51] and many-body physics. In general quantum discord is minimize with *Positive Operator Value Measurements* (POVM) instead of projective measurements as presented here, but it has been numerically found that the difference is minimal [59]. For a review see the reference [56].

1.4 Resources

The resources needed for the development of this work were a computer, books and access to the relevant literature. FONDECYT 1190727 provided both the books and the computer, iMac model 2014. The University has access to the specialized journals in digital form.

Chapter 2

Results

In this chapter we present the results of this work.

We divided their presentation in the three following sections *Hamiltonian General Properties*, *Dimer Quantum Dynamics*, *Trimer Quantum Dynamics*.

2.1 Hamiltonian General Properties

In this section we give the general properties of the model Hamiltonian

$$H = -\hbar p \sum_{i=1}^{N} (\hat{S}_i^z)^2 - \hbar J \sum_{i=1}^{N-1} (\hat{S}_i^x \hat{S}_{i+1}^x + \hat{S}_i^y \hat{S}_{i+1}^y).$$

We highlight the competition between the local anisotropy term, and the interaction term given by the XY-spin interaction. Thus, the emerging dynamics will depend on the ratio J/p.

2.1.1 Conserved spin quantities

The conserved quantities of the system are the global $\hat{S}_z$ and the total square spin of the chain $\hat{S}^2 = (\hat{S}^x)^2 + (\hat{S}^y)^2 + (\hat{S}^z)^2$,

$$\Big[\hat{S}^z, H\Big] = 0, \qquad \Big[\hat{S}^2, H\Big] = 0. \tag{2.1.1.1}$$

The rest of spin observables are in general not conserved:

$$\begin{aligned} &\Big[\hat{S}^\alpha, H\Big] \neq 0 \quad \text{with} \quad \alpha = x, y; \\ &\Big[(\hat{S}^\alpha)^2, H\Big] \neq 0 \quad \text{with} \quad \alpha = x, y, z. \end{aligned} \tag{2.1.1.2}$$

2.1.2 Unitary symmetry

The system Hamiltonian has $U(1)$ symmetry, which corresponds to the invariance of the system under global unitary rotations over the z-axis. This is proved by showing the invariance of the Hamiltonian under the following unitary transformation [39]

$$(U_\theta^z)^\dagger H U_\theta^z = H, \quad \text{with} \quad U_\theta^z \equiv \exp\Big(-i\theta \hat{S}^z\Big) = \prod_{i=1}^{N} \exp\Big(-i\theta \hat{S}_i^z\Big). \tag{2.1.2.1}$$

It can be shown that the same invariance does not hold for U_θ^α with $\alpha = x, y$.

2.1.3 Parity

As the Parity operator is unitary it follows that the system has *parity symmetry* as the Hamiltonian is invariant under the transformation

$$\Pi H \Pi = H. \tag{2.1.3.1}$$

This implies that if the initial state of the system is an eigenstate of the parity operator with eigenvalue $+1$ or -1, the system will only explore the positive or negative subspace respectively.

The proofs of all conserved quantities are presented in the appendix *Proofs*.

2.2 Dimer Quantum Dynamics

In this section we study the dynamical properties of the XY-spin-1 model for $N = 2$ particles. Being the simplest possible case where a non-trivial dynamics emerges, physical intuition is gained by its study. In particular, we discuss the effective Hamiltonian and accesible states, analytical solution, eigenstates and eigenfrequencies, evolution of the accessible states probabilities, Loschmidt echo, spin-z correlations and the von Neumann entropy evolution and its time average

2.2.1 Accessible Hilbert Space and Effective Hamiltonian

The accessible states of the system are the positive eigenstates of the Parity operator with an expectation value of the global spin-z operator $\langle \hat{S}^z \rangle = 0$:

$$\begin{aligned} |\psi_0\rangle &\equiv |00\rangle \equiv \begin{pmatrix} 1 \\ 0 \end{pmatrix}, \\ |\psi_1\rangle &\equiv (|+1,-1\rangle + |-1,+1\rangle)/\sqrt{2} \equiv \begin{pmatrix} 0 \\ 1 \end{pmatrix}. \end{aligned} \tag{2.2.1.1}$$

Where $|\psi_0\rangle$ corresponds to the initial state. In the basis $\{|\psi_0\rangle, |\psi_1\rangle\}$ the effective Hamiltonian is

$$H_{\text{eff}} = \begin{pmatrix} 0 & -\sqrt{2}J \\ -\sqrt{2}J & -2p \end{pmatrix}. \tag{2.2.1.2}$$

The emerging dynamics between the two effective states are equivalent to those of a two-level system where the initial state is a linear combination of the ground and excited states. The state of the system at time t reads

$$|\psi(t)\rangle = e^{-iE_0 t} c_{00} |E_0\rangle + e^{-iE_1 t} c_{10} |E_1\rangle, \quad \text{with} \quad c_{ij} \equiv \langle E_i | \psi_j \rangle . \tag{2.2.1.3}$$

Here, $E_0 = p(-\gamma - 1)$ and $E_1 = p(\gamma - 1)$, with $\gamma \equiv \sqrt{2(J/p)^2 + 1}$, are the eigenfrequencies of the effective Hamiltonian and $|E_0\rangle, |E_1\rangle$ their corresponding eigenstates. Therefore, the evolution of the system is periodic $|\psi(t+T)\rangle = |\psi(t)\rangle$, with period $T = \pi/p\gamma$.

2.2.2 States and Observables Evolution

In our search for signatures of dynamical quantum phase transitions (DQPTs), we study the Loschmidt echo $\mathcal{L}(t) \equiv |\langle \psi(t) | \psi_0 \rangle|^2$ since DQPTs are characterized by non-analicities in the the rate function $\lambda(t) \equiv -\ln(\mathcal{L}(t))/2$ [34, 60]. We also study the longitudinal spin alignment $A \equiv 2 - 3\langle \hat{S}^z \rangle$. This quantity was the main observable recorded in the experimental evolution studied in the Ref. [33]. As we show below and in the following subsections, A can be used to measure both the Loschmidt echo and the two-point spin-z correlation function. It can also be used to determine the time t at which a maximally entangled state is reach.

Using the effective Hamiltonian 2.2.1.2 the evolution was solved analytically. In the basis of the accessible states, the state of the system as a function of t is given by

$$|\psi(t)\rangle = \begin{pmatrix} \cos(\gamma t p) - i\frac{\sin(\gamma t p)}{\gamma} \\ i\frac{\sqrt{2}}{\gamma}\frac{J}{p}\sin(\gamma t p) \end{pmatrix}. \tag{2.2.2.1}$$

The Loschmidt echo and the probability amplitude $|c_1(t)|^2 \equiv |\langle \psi_1 | \psi(t) \rangle|^2$ are given by

$$\mathcal{L}(t) = 1 - \left(\frac{\gamma^2 - 1}{\gamma^2}\right)\sin^2(\gamma t p), \qquad |c_1(t)|^2 = \frac{2J^2/p^2}{\gamma^2}\sin^2(\gamma t p). \tag{2.2.2.2}$$

This implies that the Loschmidt echo will oscillate in time between $\mathcal{L}(t) = 1$ for $t = nT$, and $\mathcal{L}(t) = 1/\gamma^2$ for $t = (n+1)T/2$ with $n \in \mathbf{N}$. For finite values of J/p, $1/\gamma^2$ is never zero. Thus, it follows that non-analiticities never show up in the rate function $\lambda(t)$.

The longitudinal spin alignment A at time t reads

$$A = 2 - \frac{6J^2}{p^2\gamma^2}\sin^2(\gamma t p), \tag{2.2.2.3}$$

which implies that A will oscillate periodically in time between $A(t) = 2$ for $t = nT$ and $A(t) = 2 - 6J^2/p^2\gamma^2$ for $t = (n+1)T/2$ with $n \in \mathbf{N}$. When $|\psi(t)\rangle = c_0\,|\psi_0\rangle + c_1\,|\psi_1\rangle$ with $|c_0|^2 = 1/3, |c_1|^2 = 2/3$, A is equal to zero since the spin-z distribution in this state is entirely random. A reaches its minimum value, $A_{\min}$, at half-period, and several minimum values of $A_{\min}$ can be reach at different values of J/p. For instance, at $J/p = 1$, $A_{\min} = 0$. For $J/p > 1$, $A_{\min} < 0$ and reaches the minimal possible value $A_{\min} = -1$ in the limit $J/p \to \infty$. As $\mathcal{L}(t) = (A+1)/3$, the Loschmidt echo becomes zero at half-period only in the asymptotic limit $J/p \to \infty$. Therefore, signatures of a dynamical quantum phase transition are not found in the dynamics for finite values of J/p. In figure 2.1 we show the evolution of A as a function of time for values of $J/p \approx 0.23, 1.00, 4.57$.

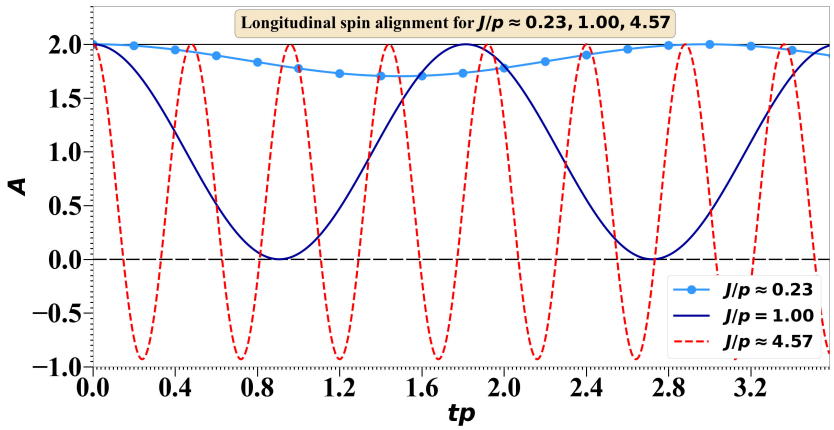

Figure 2.1: The longitudinal spin alignment A is plotted as a function of time. The lines solid with circular markers, solid, and dashed correspond to $J/p \approx 0.23, 1.00, 4.57$ respectively.

2.2.3 Spin-z Correlations

One of the main objectives of this work is to identify an adequate order parameter for describing dynamical quantum phase transitions. In general, an order parameter is such that it vanishes for one dynamical phase and takes a finite or even unbounded value in another phase in the long-time dynamics [16, 61]. With this in mind, we study the average over a period $T = \pi/p\gamma$ of the two-point spin-z correlation function $\overline{C(t)}$ for each value of J/p, which exactly reflects the desired dynamical behavior of an order parameter.

Within the framework of the effective Hamiltonian 2.2.1.2, the time average of the two-point spin-z correlation function $\overline{C(t)}$ reads

$$\overline{C(t)} \equiv \overline{\left\langle \hat{S}_1^z \hat{S}_2^z \right\rangle - \left\langle \hat{S}_1^z \right\rangle \left\langle \hat{S}_2^z \right\rangle} \equiv \frac{1}{T}\int_0^T \left[\left\langle \hat{S}_1^z \hat{S}_2^z \right\rangle - \left\langle \hat{S}_1^z \right\rangle \left\langle \hat{S}_2^z \right\rangle\right] dt = -\frac{J^2}{p^2\gamma^2}. \tag{2.2.3.1}$$

We notice that the time average of the two-point spin-z correlation is related to the longitudinal spin alignment according to the relation $\overline{C(t)} = -\overline{\langle(\hat{S}^z)^2\rangle} = (\overline{A} - 2)/3$. Therefore, in the dimer case, the average of the longitudinal spin alignment A over a period T gives the same information about the dynamics as $\overline{C(t)}$.

In figure 2.2 we plot $\overline{C(t)}$ and its derivative with respect to $\log(J/p)$. The inflection points of its first derivative are $\log(J/p) = -0.44, 0.13 \to J/p \approx 0.36, 1.45$. These points allow us to identify three dynamical

regimes. A local-dominant regime where the anisotropy term dominates the dynamics and a small close to zero time average of the two-point spin-z correlation is build. An intermediate regime where the time average of the two-point spin-z correlation quickly decreases as J/p increases, and an interaction-dominant regime where the two-point spin-z correlation time average converges towards $-1/2$. Although these points allow us to identify three dynamical regimes, we stress that the inflection points of the first derivative of the von Neumann entropy will allow us to identify finer and richer dynamical features, as we shall see in the next subsection *Von Neumann Entropy*.

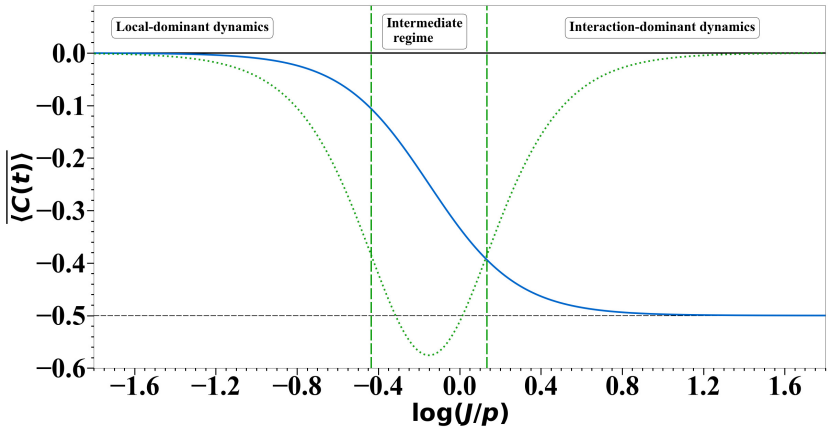

Figure 2.2: The $\log(J/p)$ is taken in base 10. The solid (blue) line represents $\overline{C(t)}$ averaged over $T = \pi/p\gamma$ as function of $\log(J/p)$. The dotted (green) line shows the first derivative of the time average $\overline{C(t)}'$ with respect to $\log(J/p)$ scaled by 1/5 to fit the plot. The solid (black) horizontal line is set at 0 which is the value of $\overline{C(t)}$ in the limit $J/p \to 0$. The horizontal dashed line is set at $-1/2$ which is the value of $\overline{C(t)}$ in the limit $J/p \to \infty$. The vertical dashed lines are at the inflection points of $\overline{C(t)}'$, that is, $\log(J/p) = -0.44, 0.13$.

2.2.4 Von Neumann Entropy

Analytically the von Neumann entropy associated with the reduced density matrix $\rho_1(t) = \rho_2(t)$ reads

$$S(t) = -|c_0|^2 \log_3 |c_0|^2 - |c_1|^2 \log_3 \frac{|c_1|^2}{2}, \tag{2.2.4.1}$$

with $|c_0|^2 = \cos^2(\gamma t) + \sin^2(\gamma t)/\gamma^2$ and $|c_1|^2 = 2J^2 \sin^2(\gamma t)/\gamma^2 p^2$. In figure 2.3 we show the von Neumann entropy evolution as a function of time for values of $J/p \approx (0.23, 0.85, 1.78, 4.57)$. The maximum entropy, $S(t) = 1$, is reached for the maximally entangled qutrit state state $|\psi(t)\rangle = c_0 |\psi_0\rangle + c_1 |\psi_1\rangle$with $|c_0|^2 = 1/3$ and $|c_1|^2 = 2/3$. For $J/p < 1$ the system never reaches the maximum entropy. For $J/p = 1$ it reaches the maximum entropy, and therefore a maximally entangled state, once per period. For $J/p > 1$ it reaches the maximum entropy twice per period. This pattern can be clearly understood by looking at the probability amplitude of the accessible state $|\psi_1\rangle$ in eq. 2.2.2.2. During a complete period the maximum value of $|c_1|^2$ is greater than 2/3 for $J/p > 1$, and therefore the point $|c_1|^2 = 2/3$ is reached twice in each period. Due to the long time window that the dimer is nearly a maximally entangled state when $J/p \sim 1$, the dynamics provides a good protocol to generate highly entangled states of spin-1 systems.

In figure 2.4 we plot the time-average over a period $T = \pi/p\gamma$ of the von Neumann Entropy and its first derivative with respect to $\log(J/p)$. In contrast with the first derivative of the time average of the two-point spin-z correlation function $\overline{C(t)}$, we identify three inflection points of the first derivative of the time average entropy $\overline{S(t)}$ which are able to capture richer and finer dynamical features. In particular, we define four different dynamical regimes, namely, a local-dominant regime, a first intermediate regime, a second intermediate regime, and an interaction-dominant regime. These regimes are explained in the following.

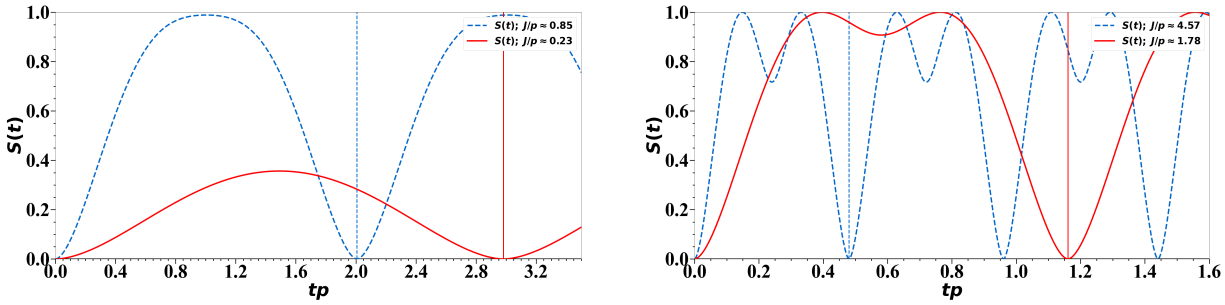

Figure 2.3: In the left panel we show the evolution of $S(t)$ for $J/p \approx 0.23, 0.85$. The vertical solid (red) and dashed (blue) line are set at the first period of evolution $T = \pi/p\gamma$ for $J/p \approx 0.23, 0, 85$ respectively. In the right panel we show the evolution of $S(t)$ for $J/p \approx 1.78, 4.57$. The vertical solid (red) and dashed (blue) lines are set at the first period of evolution $T = \pi/p\gamma$ for $J/p \approx 1.78, 4.57$ respectively.

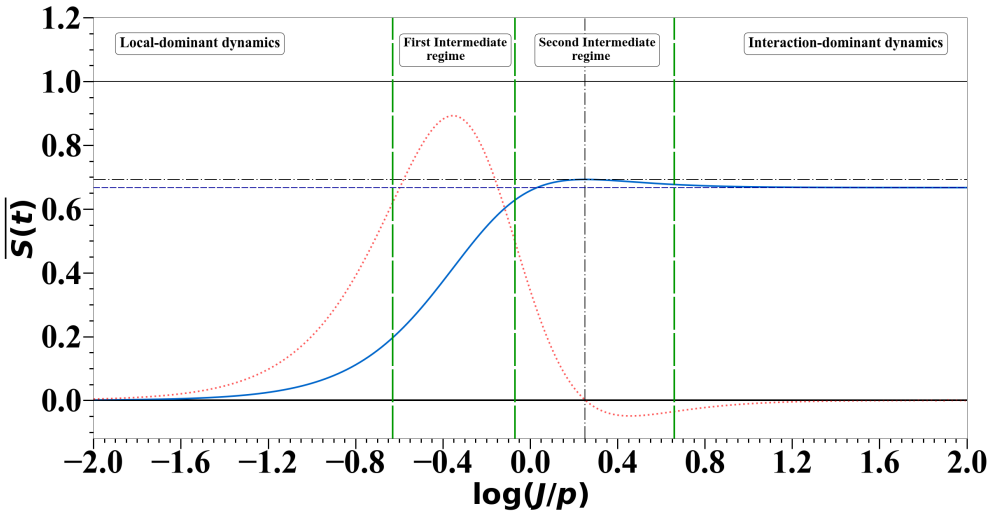

Figure 2.4: The $\log(J/p)$ is taken in base 10. The solid (blue) lines represents the average von Neumann entropy $\overline{S(t)}$ as a function of $\log(J/p)$. The dotted (red) line represents the first derivative of $\overline{S(t)}$ with respect to $\log(J/p)$, $\overline{S(t)}'$. The vertical long-dashed (green) lines are set at the inflection points of $\overline{S(t)}'$ $\log(J/p) = -0.63, -0.07, 0.66 \rightarrow J/p \approx 0.23, 0.85, 4.57$. The vertical and horizontal dashdotted (black) lines show the maximal value of $\overline{S(t)}$ reached for $\log(J/p) = 0.25 \rightarrow J/p \approx 1.78$. The horizontal short-dashed (blue) line is set at the asymptotic value of $\overline{S(t)} \approx 0.6671$ in the limit $J/p \rightarrow \infty$.

We define the local-dominant regime for $J/p < 0.23$, where we identify the first inflection point at $J/p \approx 0.23$. In this regime, $\overline{S(t)}$ slowly increases from 0 in the limit $J/p \rightarrow 0$ to $\overline{S(t)} = 0.196$ for $J/p \approx 0.23$.

We define the first intermediate regime with $J/p \in (0.23, 0.85)$, where we identify the second inflection point at $J/p \approx 0.85$. In this regime, $\overline{S(t)}$ rapidly increases from 0.196 for $J/p \approx 0.23$ to 0.628 for $J/p \approx 0.85$.

We define the second intermediate regime with $J/p \in (0.85, 4.57)$, where we identify the third inflection point at $J/p \approx 4.57$. In this regime, $\overline{S(t)}$ slowly increases until reaching a maximum $\overline{S(t)}_{max} \approx 0.693$ at $J/p \approx 1.78$, and then starts to slowly decrease.

We define the interaction-dominant regime with $J/p > 4.57$, where $\overline{S(t)}$ converges towards the asymptotic value of $\overline{S(t)} \approx 0.6671$ in the limit of $J/p \rightarrow \infty$. This diminution of the average entropy is explained by the fact that the dip between the two maximum of $S(t)$, reach at $T/2$, is more pronounced as J/p increases.

Compare the dips between the two maximum within each period for $J/p \approx 1.78$ and $J/p \approx 4.57$ in the right panel of figure 2.3.

The dip between the two maximum of the von Neumann entropy is explained as follows. In figure 2.5 we plot the von Neumann entropy 2.2.4.1 of the state $|\psi\rangle = c_0 |\psi_0\rangle + c_1 |\psi_1\rangle$ as a function of $|c_0|^2$. In the evolution, for $J/p > 1$ the von Neumann entropy will reach its maximum value of 1 when $|c_0(t)|^2 = 1/3$ at a time $t < T/2$. Then, it will decrease until $t = T/2$ when $|c_0(t)|^2$ reaches its minimal value. We indicate the minimal values reach by $|c_0(t)|^2 \equiv |\langle\psi_0|\psi(t)\rangle|^2$ with vertical solid, dashed and dotted lines for $J/p \approx 1.00, 1.78, 4.57$ respectively. As for increasing J/p the minimum value reach by $|c_0(t)|^2$ gets smaller, so does the dip between the two maximum and the average over a period decreases.

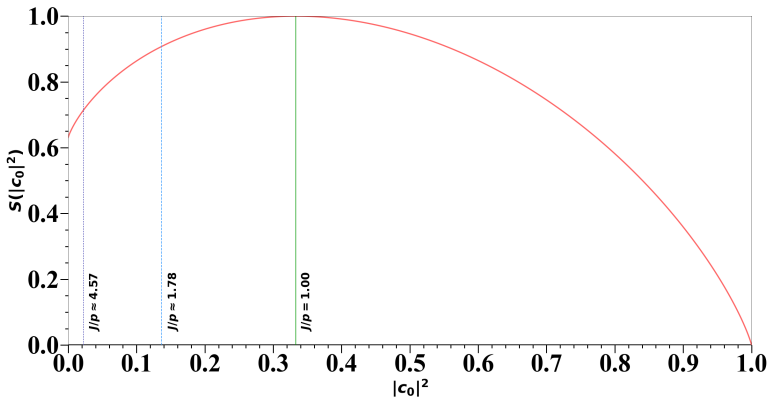

Figure 2.5: The solid (red) line shows the static von Neumann entropy as a function of $|c_0|^2$. The vertical solid, dashed and dotted lines respectively correspond to the minimum values reach by $|c_0(t)|^2 \to 1/\gamma^2$ with $\gamma = \sqrt{2J^2/p^2 + 1}$ in the evolution for values of $J/p \approx 1.00, 1.78, 4.57$.

We remark that the values of J/p given by the inflection points of the first derivative of $\overline{S(t)}$ provide a guideline to categorize and better understanding the different emerging dynamics of the system with respect to the ratio of J/p. We also conclude that the average of the von Neumann entropy is a more complete order parameter than the average of the two-point spin-z correlation function, in the sense that more information about the different emerging dynamical regimes can be extracted from it.

We further note that if a unique time T is fix to study the average over the whole J/p spectrum, then the long-time asymptotic behavior is not well represented for all values of J/p, and physical information about the dynamics is lost. For example, if a fix T throghout all the J/p spectrum is used to calculate $\overline{S(t)}$, its derivative losses its physical meaning since it would be quickly oscillating between positive and negative values. In contrast, if the average is taken over the period $T = \pi/p\gamma$ for each value of J/p, the derivative of $\overline{S(t)}$ smoothly changes as we show in the figure 2.4. For the dimer the evolution is periodic, and it is simple to determine the appropriate value of T for each value of J/p that captures the average in the asymptotic long-time limit $T \to \infty$. Finding the values of T that correctly represent the average in the asymptotic long-time limit will become more challenging as the number of sites in the lattice increases, as we will discuss in the next section.

2.3 Trimer Quantum Dynamics

In this section we study the dynamical properties of the XY-spin-1 model for $N = 3$ particles. The trimer corresponds to the smallest chain without an analytic solution for the emergent dynamics. In comparison with the dimer, we obtained richer non-periodic emerging dynamics, and additional physical intuition is gained with respect to the emerging times scales. We find signatures of a dynamical quantum phase transition, and confirm that time averaged bipartite entropies are more complete order parameters than the time average of the two-point spin-z correlation functions. Further, we study the role of the parity symmetry of the system in the mutual information distribution. In particular, we discuss the effective Hamiltonian, accesible states, eigenstates and eigenfrequencies, Loschmidt echo and its rate function, spin-z correlations, bipartite entropies, and mutual informations.

2.3.1 Effective Hamiltonian

The accessible states of the system are the positive eigenstates of the Parity operator with an $\langle \hat{S}^z \rangle = 0$:

$$
\begin{aligned}
|\psi_0\rangle &\equiv |000\rangle \equiv \begin{pmatrix} 1 \\ 0 \\ 0 \end{pmatrix}, \\
|\psi_1\rangle &\equiv (|+1,-1,0\rangle + |0,-1,+1\rangle + |-1,+1,0\rangle + |0,+1,-1\rangle)/2 \equiv \begin{pmatrix} 0 \\ 1 \\ 0 \end{pmatrix}, \\
|\psi_2\rangle &\equiv (|+1,0,-1\rangle + |-1,0,+1\rangle)/\sqrt{2} \equiv \begin{pmatrix} 0 \\ 0 \\ 1 \end{pmatrix}.
\end{aligned}
\tag{2.3.1.1}
$$

In this basis the effective Hamiltonian is

$$
H_{\text{eff}} = \begin{pmatrix} 0 & -2J & 0 \\ -2J & -2p & -\sqrt{2}J \\ 0 & -\sqrt{2}J & -2p \end{pmatrix}. \tag{2.3.1.2}
$$

The state of the system at time t reads

$$
|\psi(t)\rangle = \sum_{i=0}^{2} e^{-iE_i t} c_{i0} \, |E_i\rangle \,, \quad \text{with} \quad c_{ij} \equiv \langle E_i | \psi_j \rangle \,, \tag{2.3.1.3}
$$

where the E_i and $|E_i\rangle$ are the eigenfrequencies and eigenstates of the effective Hamiltonian.

At time t the probability amplitudes $p_i \equiv |\, \langle \psi_i | \psi(t) \rangle \,|^2$ of the accessible states read

$$
|\, \langle \psi_i | \psi(t) \rangle \,|^2 = \left| \sum_{j=0}^{2} c_{ji}^{*} c_{j0} e^{-iE_j t} \right|^2 , \tag{2.3.1.4}
$$

and the expectation value of any observable $\hat{O}$ reads

$$
\left\langle \hat{O} \right\rangle = \sum_{i,j=0}^{2} c_{i0}^{*} c_{j0} \, \langle E_i | \hat{O} | E_j \rangle \, e^{-i\Delta_{ji} t}, \quad \text{with} \quad \Delta_{ij} \equiv E_i - E_j. \tag{2.3.1.5}
$$

Is clear that all the emerging dynamics are, at least in principle, contained in the accessible states, eigenstates and eigenfrequencies of the system. Therefore, for characterizing the emerging dynamics it is useful to study the spectral properties of the frequencies (or energies) of the system [62, 63]. In our particular finite case, the ratio between frequencies $R_f \equiv \min(\Delta_{21}/\Delta_{10}, \Delta_{10}/\Delta_{21})$ will determine the time scales of the dynamics.

Commensurable values of R_f will lead to periodic dynamics, and uncommesurable values of R_f will lead to non-periodic dynamics. We numerically find that for $J/p \neq 0, \infty$ R_f is always uncommesurable, and the emerging dynamics will always be non-periodic. In figure 2.6 we plot R_f, and the weights of the effective Hamiltonian eigenstates, $|c_{ij}|^2$, in the initial state as a function of $\log(J/p)$. We discuss their relation with the emerging dynamics in the appendix *Trimer Additional Results*.

In figure 2.6 the values $\log(J/p) = -0.73, 0.65, -0.2, -0.11, 0.67 \rightarrow J/p \approx 0.19, 0.22, 0.63, 0.78, 4.68$ correspond to the inflection points of the first derivatives of the averaged bipartite entropies $\overline{S_{12-3}(t)}$ and $\overline{S_{13-2}(t)}$ with respect to $\log(J/p)$. As in the dimer, these points allow us to define four different dynamical regimes, as we further discuss below in *States and Observables Evolution* and *Bipartite Entropies*. We show these points in figure 2.6 to highlight how the dynamical regimes that we identify for the trimer are consistent with the behavior of both R_f and the weights $|c_{i0}|^2$.

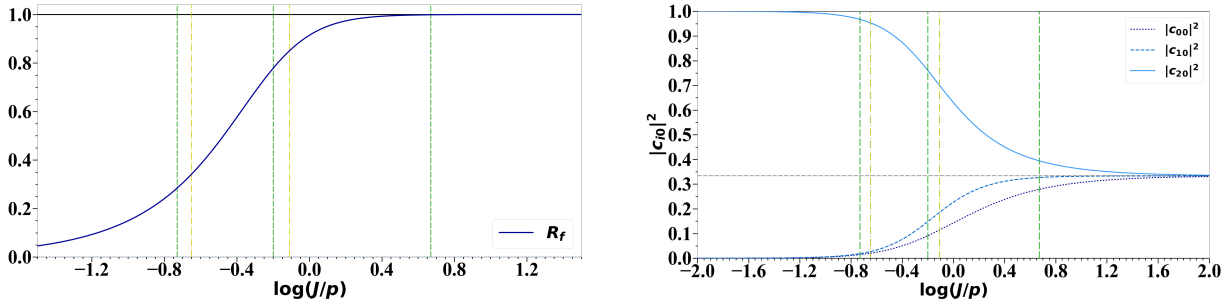

Figure 2.6: The $\log(J/p)$ is taken in base 10. The left panel shows R_f as a function of $\log(J/p)$. The right panel shows the weights of the effective Hamiltonian eigenstates in the initial state plotted as a function of $\log(J/p)$. In the right panel the dashed horizontal line is set at 1/3. The weights $|c_{00}|^2$ and $|c_{10}|^2$ steadily increase in the intermediate regime $\log(J/p) \in (-0,73, .67)$ from 0.0144 and 0.0184 to 0.2788 and 0.3267 respectively, which are close to their asymptotic values $|c_{00}|^2 = |c_{10}|^2 = |c_{20}|^2 = 1/3$ in the limit $J/p \rightarrow \infty$. In both panels the dashdotted (yellow) and dashed (green) vertical lines mark the inflection points of the first derivatives of $\overline{S_{12-3}(t)}$ and $\overline{S_{13-2}(t)}$ respectively.

2.3.2 States and Observables Evolution

In figure 2.7 we plot the short time evolution of probability amplitudes of the accessible states for values of $J/p \approx 0.19, 0.78, 2.19, 4.68$. As expected from the effective Hamiltonian (2.3.1.2) structure, initially in the evolution $p_1 \equiv |\langle\psi_1|\psi(t)\rangle|^2$ increases while $p_2 \equiv |\langle\psi_2|\psi(t)\rangle|^2$ remains close to zero. Afterwards all three probabilities will in general oscillate non-periodically.

For $J/p < 0.19$, in the local-dominant regime, the system slightly departs from the initial state to then come back to it quasi-periodically.

In the intermediate regime, $0.19 < J/p < 4.68$, the system oscillates away from the initial state until it reaches a minimal value of the Loschmidt echo, $\mathcal{L}(t)$, and then starts returning to the initial state, completing a Poincare Recurrence at a time T_r (see the left panel of figure 2.8). This is a finite-size effect of the system, and for larger systems this observable Poincare recurrence will occur in longer times.

The value of $J/p = 1.00$ establishes a relevant point which allows us to differentiate a true Poincare recurrence from a near return to the initial state at time T_m. For $J/p < 1.00$, $T_m = T_r$. For $J/p > 1.00$ $T_m \neq T_r$. For example, in the lower right panel of 2.7, the solid (blue) line shows the short time evolution of $\mathcal{L}(t) \equiv |\langle\psi_0|\psi_(t)\rangle|^2$. In this short times we see a quasi-periodic evolution with period T_m. This quasi-periodic evolution is lost in longer times which we show in the right panel of figure 2.8. There, we can see that that the system drifts away from the initial state until finite size effects dominate the dynamics and a Poincare recurrence occurs. See the appendix *Trimer Additional Results* for a plot of T_r, T_m, and a discussion of their connection with the eigenfrequencies of the system.

In the intermediate regime $0.19 < J/p < 4.68$ the minimum value reached by $\mathcal{L}(t)$ gradually decreases from approximately 0.87 for $J/p \approx 0.19$ to be lower than 0.001 for $J/p \approx 1.66$. For all the values of $J/p > 1.66$ the

rate function $\lambda(t) \equiv -\ln(\mathcal{L}(t))/3$ has clear kinks at the times where the fidelity is lowest, showing signatures of a dynamical quantum phase transition with a critical point in $J/p \approx 1.66$. For smaller values of J/p these kinks become less pronounced. For example, for $J/p = 1.00$ the rate function has no kinks whatsoever. In figure 2.9 we show the evolution of the rate function for $J/p \approx 1.00, 1.66$.

Crucially, in contrast to what happened in the 1-D Transverse Field Ising Model (TFIM) studied in [38], where only for certain discrete values of the quench parameters the system evolved towards an orthogonal state with respect to the initial state, in our spin-1 model for all values of $J/p > 1.66$ the system evolves towards an almost completely orthogonal state $|\psi'(t)\rangle$ with respect to the initial state (i.e. $|\langle\psi'(t)|\psi_0\rangle|^2 < 0.001$). In the appendix *Trimer Additional Results* we give a plot showing the minimal values reach by $\mathcal{L}(t)$. We also discussed there how the longitudinal spin alignment can be used to measure the Loshcmidt echo.

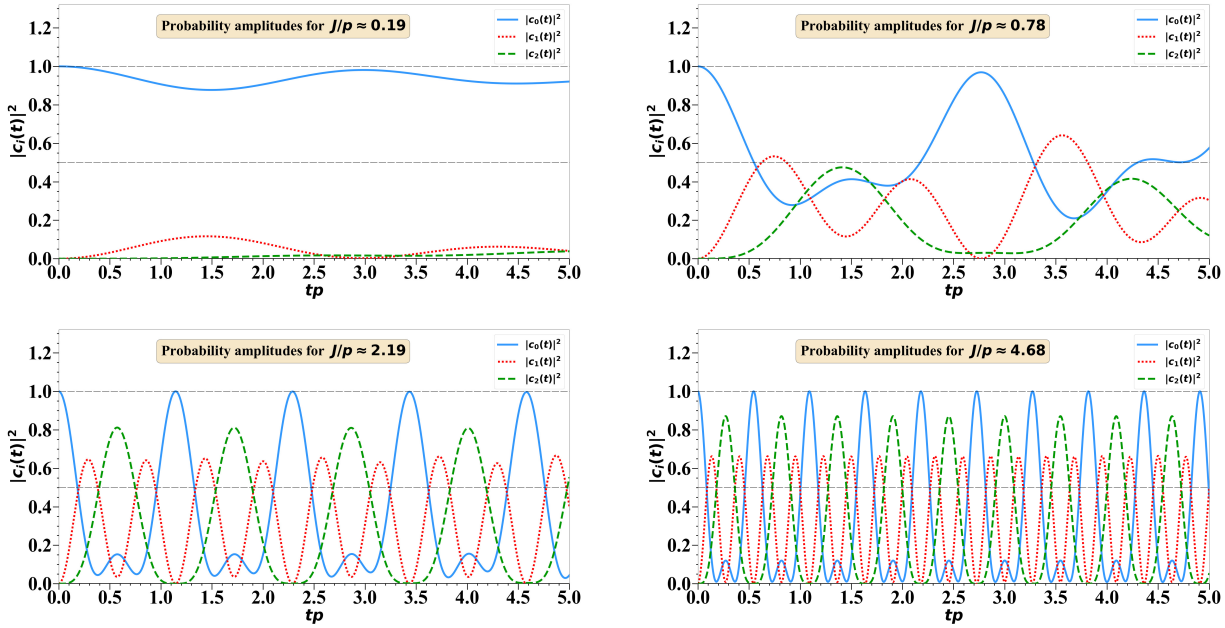

Figure 2.7: From left to right and up to down the panels show the probability amplitudes as a function of time for the accessible states in the system evolution for values of $\log(J/p) = -0.73, -0.11, 0.34, 0.67 \rightarrow J/p \approx 0.19, 0.78, 2.19, 4.68$. In the labels $|c_i(t)|^2| \equiv |\langle\psi_i|\psi(t)\rangle|^2$.

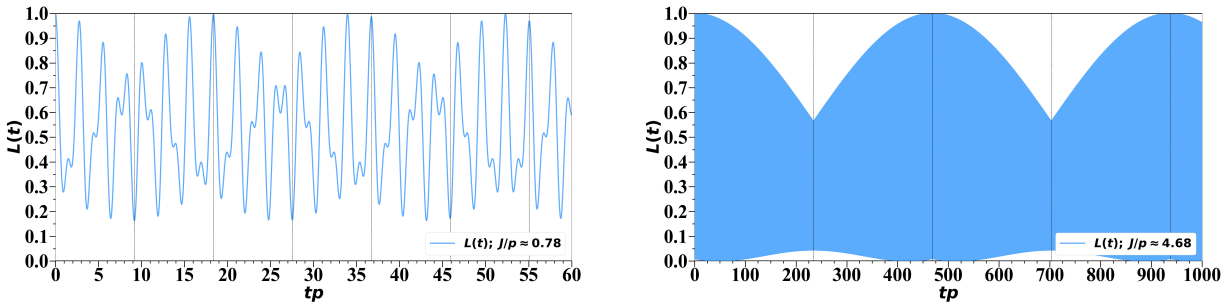

Figure 2.8: The left (right) panel shows the Loschmidt echo $\mathcal{L}(t)$ for $J/p \approx 0.78$ ($J/p \approx 4.68$). In the left panel the vertical dashed lines are half-integers multiples of the the first Poincare recurrence time $T_r \approx 18.34p^{-1}$. When $t = T_r$ $\mathcal{L}(t) \approx 0.997$. The second recurrence time is shorter than the first. The half-integers multiples of the first recurrence time coincide with local maxima and minima in the fidelity due to the quasi-periodic nature of the evolution. For longer times this coincidence is broken. In the right panel the vertical dashed lines are half-integer multiples of the the first Poincare recurrence time $T_r \approx 469.55p^{-1}$. Due to the long time shown and its rapid oscillation the line for $\mathcal{L}(t)$ looks like is filling all the colored region but is not.

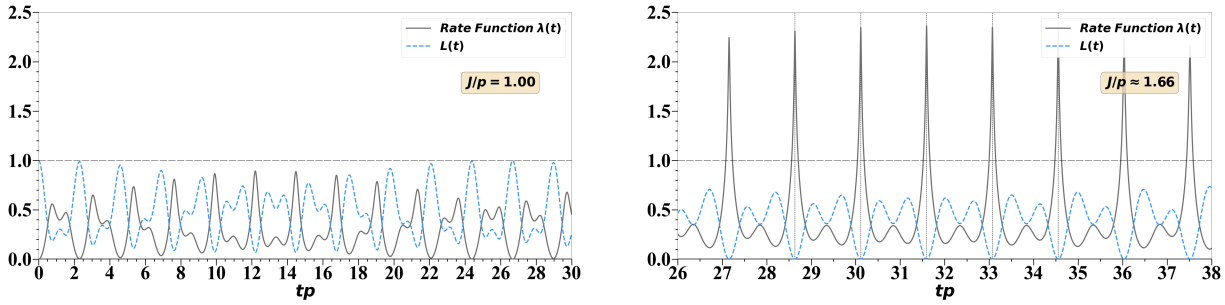

Figure 2.9: The left panel shows the Loschmidt echo $\mathcal{L}(t)$ and the rate function $\lambda(t)$ as functions of time for $J/p = 1.00$. The right panel shows the Loschmidt echo $\mathcal{L}(t)$ and the rate function $\lambda(t)$ as functions of time for $J/p \approx 1.66$. The dashed vertical lines are set at the peaks of the rate function which signal a Loschmidt echo $\mathcal{L}(t) < 0.001$. In the right panel the plot is centered around $T_r/2 \approx 31.6$ which is very close, but not exactly equal, to the time in which $\lambda(t)$ is highest.

2.3.3 Spin-z Correlations

For the trimer there are two different two-point spin-z correlation functions

$$C_{12}(t) = \left\langle \hat{S}_1^z \hat{S}_2^z \right\rangle - \left\langle \hat{S}_1^z \right\rangle \left\langle \hat{S}_2^z \right\rangle \quad \text{and} \quad C_{13}(t) \equiv \left\langle \hat{S}_1^z \hat{S}_3^z \right\rangle - \left\langle \hat{S}_1^z \right\rangle \left\langle \hat{S}_3^z \right\rangle . \tag{2.3.3.1}$$

In our specific dynamics these correlations time averages are given by

$$\overline{C_{12}(t)} = \overline{-|c_1(t)|^2/2}, \qquad \overline{C_{13}(t)} = \overline{-|c_2(t)|^2}. \tag{2.3.3.2}$$

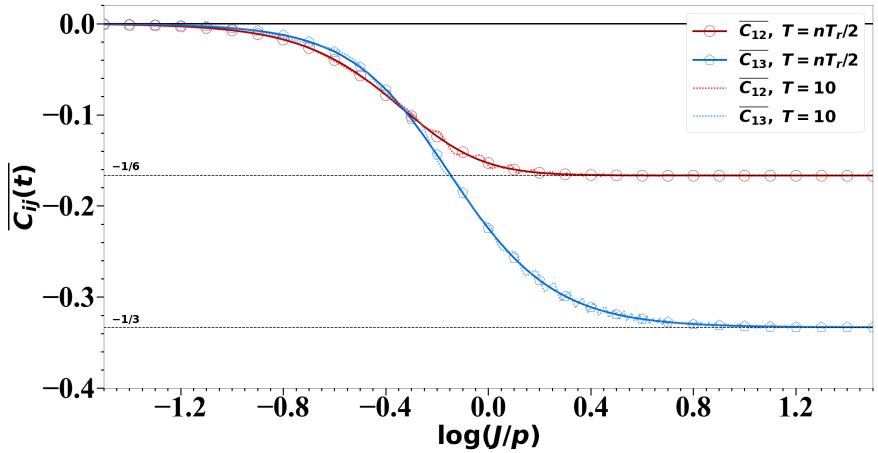

Figure 2.10: The $\log(J/p)$ is taken in base 10 and is shown with a step of 0.01 between points. The solid lines show the two-point spin-z correlation functions $\overline{C_{12}(t)}$ and $\overline{C_{13}(t)}$ averaged over integer multiples of the half-recurrence times $nT_r/2$ for each value of $\log(J/p)$. We choose different decreasing values of n between 80 for $J/p < 1.00$ and 1 for $J/p > 25$, this implies that the integration times $nT_r/2$ approximately ranged between 252 p^{-1} for $J/p \approx 0.04$ to 6700 p^{-1} for $J/p \approx 25.12$. The dotted lines show $\overline{C_{12}(t)}$ and $\overline{C_{13}(t)}$ averaged over a fix value of $T = 10$ for each value of $\log(J/p)$. The horizontal dashed lines are set at $-1/3$ and $-1/6$.

In figure 2.10 we plot the two-point spin-z correlation functions time average over integer multiples of the half-recurrence times $T_r/2$ for each value of $\log(J/p)$. Their first-derivatives inflection points identify an intermediate regime but not as precisely as bipartite entropies and we omit showing them. We also plot

their time average over an unique constant cutoff $T = 10\ p^{-1}$ for each value of $\log(J/p)$. In the interaction-dominant regime the averages over both short and long times of $\overline{C_{12}(t)}$ and $\overline{C_{13}(t)}$ converge towards $-1/6$ and $-1/3$ respectively. In the intermediate regime the short time average oscillates around the average in the recurrence times. This implies that the predicted Poincare recurrences and the overall behavior of the dynamics are not well trapped by the average of the two-point spin-z correlation functions, as there is no substantial difference between the short time averages and the recurrence time averages. Nonetheless, in the intermediate regime the evolution of both $C_{12}(t)$ and $C_{13}(t)$ reflect the overall behavior and the Poincare recurrences of the system. In the appendix *Trimer Additional Results* we further discuss the long time evolution of $C_{12}(t)$ and $C_{13}(t)$.

We note that for any fix T, that is not extremely long, the oscillations seen in the average when $T = 10\ p^{-1}$ are unavoidable due to the different time scales of the emerging dynamics for the different values of J/p. We stress that these oscillations in the averages, when the average is taken for a short fix T throughout all the J/p spectrum, do not carry any significant physical information.

2.3.4 Bipartite Entropies

The bipartite entropies $S_{12-3}(t)$ and $S_{13-2}(t)$ are

$$S_{12-3}(t) = S(\rho_3(t)) = -(|c_1(t)|^2/2 + |c_2(t)|^2)\log\left(\frac{|c_1(t)|^2/2 + |c_2(t)|^2}{2}\right) - \left(|c_0(t)|^2 + |c_1(t)|^2/2\right)\log\left(|c_0(t)|^2 + |c_1(t)|^2/2\right), \tag{2.3.4.1}$$

$$S_{13-2}(t) = S(\rho_2(t)) = -|c_1(t)|^2\log\left(\frac{|c_1(t)|^2}{2(1-|c_1(t)|^2)}\right) - \log\left(1-|c_1(t)|^2\right). \tag{2.3.4.2}$$

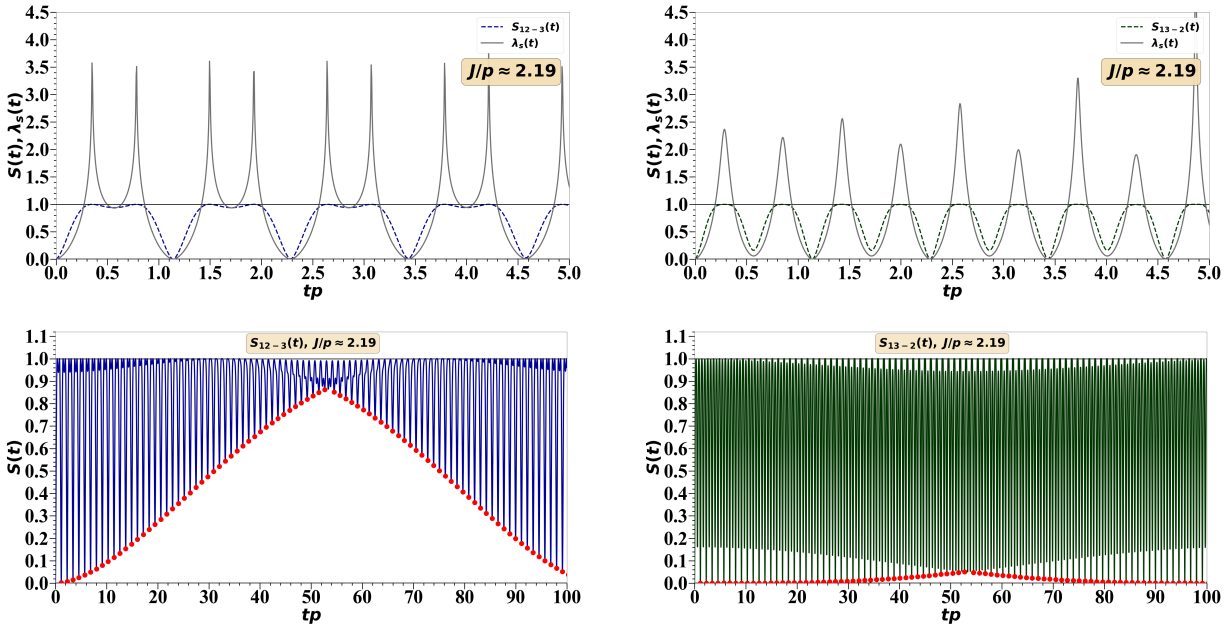

Figure 2.11: The upper left (right) panel shows the short time evolution of $S_{12-3}(t)$ ($S_{13-2}(t)$) for $J/p \approx 2.19$. The lower left (right) panels show the long time evolution of $S_{12-3}(t)$ ($S_{13-2}(t)$) for $J/p \approx 2.19$.

In figure 2.11 we show the long and short time evolution of $S_{12-3}(t)$ and $S_{13-2}(t)$ for $J/p \approx 2.19$. We remark that the lowest value of J/p at which $S_{12-3}(t)$ reaches a value higher than 0.999 is $J/p = 1.00$, which is the same value of J/p such that the maximum entropy is reach in the dimer. In the appendix *Trimer Additional Results* we give a plot showing the maximal values reach by the bipartite entropies as a function of $\log(J/p)$.

In the lower panels of figure 2.11 we highlight with circular red markers the minimal values of $S_{12-3}(t)$ and $S_{13-2}(t)$ within each quasi-period T_m. The time at which this minima change from increasing to decreasing is when finite size effects start to dominate the dynamics. This is very clear in the evolution of $S_{12-3}(t)$, see the lower left panel. Notice that the behavior of $S_{13-2}(t)$ is different from the behavior of $S_{12-3}(t)$, see the lower right panel. We interpret their different behavior in terms of mutual information and the parity symmetry of the system below in *Mutual Information*. See the appendix *Trimer Additional Results* for plots off the long time evolution with other values of J/p.

In figure 2.12 we show the time averages $\overline{S_{13-2}(t)}$ and $\overline{S_{12-3}(t)}$ for a fix time $T = 10\ p^{-1}$ for all values of $\log(J/p)$. We also show the time averages taken over integer multiples of half-recurrence times $T_r/2$ for each value of $\log(J/p)$. In contrast to the spin-z correlations, the time averages of the bipartite entropies clearly reflect the overall evolution and Poincare recurrences of the dynamics, as shown by the large difference between the averages taken for a fix T throughout the whole J/p spectrum, and the averages taken over the recurrence times. The classification of the different emerging dynamical regimes is more complete and richer when the averages are taken over the Poincare recurrence times instead of an arbitrary value T. In other words, we need to identify the times at which finite-size effects enter the dynamics and ruled them out. We stress that this is one of the main results of this thesis.

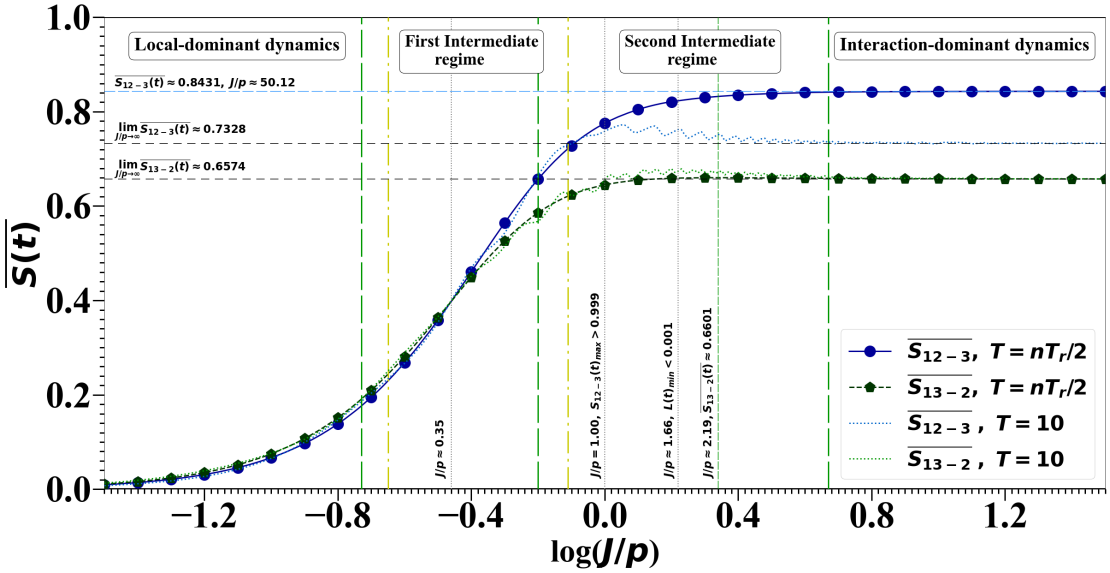

Figure 2.12: The $\log(J/p)$ is taken in base 10. The averages over $nT_r/2$ were calculated for all values of $\log(J/p) \in (-2, 1.7)$ with a step of 0.01. We choose different decreasing values of n between 80 for $J/p < 1.00$ and 1 for $J/p > 25$, this implies that the integration times $nT_r/2$ approximately ranged between 252 p^{-1} for $J/p \approx 0.04$ to 6700 p^{-1} for $J/p \approx 25.12$. The vertical dashed (green) and dashdotted (yellow) lines are set at the inflection points of $\overline{S_{13-2}(t)}'$ and $\overline{S_{12-3}(t)}'$ respectively. The recurrence times were manually identified for all values of $\log(J/p)$ between 0.2 and 1.7 with a step of 0.05. For the calculation of the time average entropies, the Poincare recurrence times T_r were obtained from an exponential fit of the manually obtain values. We show a plot with the exponential fitting of the T_r times in the appendix *Trimer Additional Results*. Although the curves for the averages $\overline{S_{12-3}(t)}$ and $\overline{S_{13-2}(t)}$ appear smooth, numerically their derivatives were discontinuous at all points. We deemed this discontinuities as non-physical. To calculate the inflection points of the derivatives the numerical data was fitted to a polynomial using the NUMPY built-in package Polynomial.

In figure 2.12 the vertical dashdotted (yellow) and dashed (green) lines are set at the inflection points of the first derivative with respect to $\log(J/p)$ of the averages $\overline{S_{12-3}(t)}$ and $\overline{S_{13-2}(t)}$ taken over the recurrence times T_r which are, respectively, $\log(J/p) = -0.65, -0.11, \rightarrow J/p \approx 0.22, 0.78$ and $\log(J/p) = -0.73, -0.20, 0.67 \rightarrow J/p \approx 0.19, 0.63, 4.68$. These points allow us to define four different dynamical regimes similar to the ones defined in the dimer.

We define the local-dominant regime for $J/p < 0.19$, where we identify the first inflection point of $\overline{S_{13-2}(t)}'$. In this regime, the system evolves near the initial state and the entropies are small at all times with $\overline{S_{13-2}(t)}$ being slightly larger than $\overline{S_{12-3}(t)}$.

We define the first intermediate-regime, $J/p \in (0.19, 0.78)$, where we identify the second inflection point of $\overline{S_{12-3}(t)}'$ at $J/p \approx 0.78$. Makes no difference to the following discussion to define the first-intermediate regime with $J/p \in (0.19, 0.63)$, where we identify the second inflection point of $\overline{S_{13-2}(t)}'$ at $J/p \approx 0.63$. In this regime, the time average bipartite entropies increase very rapidly as J/p increases. An important point in this transition regime occurs at $\log(J/p) = -0.46 \to J/p \approx 0.35$. Here, the time average $\overline{S_{12-3}(t)}$ becomes larger than $\overline{S_{13-2(t)}}$. We comment on the interpretation of this point below in *Mutual Information*.

We define the second intermediate regime, $J/p \in (0.78, 4.68)$, where we identify the third inflection point of $\overline{S_{13-2}(t)}'$ at $J/p \approx 4.68$. In this regime, $\overline{S_{13-2}(t)}$ stabilizes near its asymptotic value reaching its maximum at $J/p \approx 2.19$. The $\overline{S_{12-3}(t)}$ continues to increase, albeit more slowly than in the first intermediate regime, towards its value in the interaction-dominant regime defined below. Important points in this regime are $\log(J/p) = 0.22 \to J/p \approx 1.66$ and $\log(J/p) = 0.00 \to J/p = 1.00$. The value $J/p \approx 1.66$ is the minimal value where signatures of a dynamical quantum phase transition appear in the dynamics. The value $J/p \approx 1.00$ is the minimal ratio where the maximum of $S_{12-3}(t)$ is higher than 0.999.

We define the interaction-dominant regime for $J/p > 4.68$. In this case, the averages of the entropies stabilize and remain very close to the ones given at $J/p \approx 4.68$. To highlight this, in figure 2.12 we plotted the horizontal dashed (light blue) line at the value of $\overline{S_{12-3}(t)}$ averaged over its recurrence time for a large $J/p \approx 50.12$ approaching the asymptotic limit within the limitations of our numerical calculation, which we find is very similar to the one obtained for $J/p \approx 4.68$.

We remark that the averages in the interaction-dominant regime of $\overline{S_{12-3}(t)}$ over the recurrence times are much higher than the average entropy obtained in the limit $J/p \to \infty$ $\overline{S_{12-3}(t)} \approx 0.7328$. On the other hand, the time averages $\overline{S_{12-3}(t)}$ for a fix $T = 10\ p^{-1}$ for all values of J/p seem to indicate that in the interaction-dominant regime $\overline{S_{12-3}(t)}$ converges towards this asymptotic value $\overline{S_{12-3}(t)} \approx 0.7328$. This is due to the fact that the quasi-periodic evolution at short times resembles the periodic evolution of the system in the limit $J/p \to \infty$. Further, these short time averages also seem to indicate that a higher bipartite entropy is build on average in the intermediate regime. This is so because in the intermediate regime the system quickly departs from the initial state, and low entropy states disappear from the dynamics until finite size effects dominate the dynamics (see the lower left panel of figure 2.11).

For the above stated reasons, and to avoid non-physical fluctuations in the time average of relevant quantities, we stress the importance of identifying the half-recurrence times at which finite-size effects start to dominate the dynamics for all ratios of J/p. We also remark that simply choosing a longer arbitrary time T is not enough to avoid the non-physical fluctuations in the averages and appropriately capture the long time asymptotic averages $T \to \infty$. Further, studying the time average over the Poincare recurrence times of the bipartite entropies allow us to obtained a more complete and richer classification of the emerging dynamics in comparison with the time averages of the two-point spin-z correlation functions.

In the appendix *Trimer Additional Results* we provide a plot showing the bipartite entropy averages for values of $T = 20, 50, 100, 1000$.

2.3.5 Mutual Information

In order to give a correct interpretation of the behavior of $\overline{S_{12-3}(t)}$ and $\overline{S_{13-2}(t)}$ seen in the lower panels of figure 2.11, we study the mutual informations I_{12}, I_{13} and I_{1-23} which by definition are

$$\begin{aligned} I_{12}(t) &= S_1(t) + S_2(t) - S_{12}(t), \\ I_{13}(t) &= S_1(t) + S_3(t) - S_{13}(t), \\ I_{1-23}(t) &= S_1(t) + S_{23}(t) - S(t) \end{aligned} \tag{2.3.5.1}$$

where $S_i(t) \equiv S(\rho_i(t)), S_{ij}(t) \equiv S(\rho_{ij}(t))$ and $S(t) \equiv S(\rho(t))$ is the von Neumann entropy of the system, and $\rho_{ij}(t), \rho_i(t)$ are the corresponding reduced density matrices. As the state of the system is pure at all times it holds that $S_{12-3}(t) = S_3(t) = S_{12}(t)$ and $S_{13-2}(t) = S_2(t) = S_{13}(t)$. From the parity symmetry of the system it also holds that $S_1(t) = S_3(t)$. Therefore, the following relations between mutual informations and bipartite entropies hold:

$$S_{13-2}(t) = I_{12}(t), \quad \text{and} \quad S_{12-3}(t) = (I_{12}(t) + I_{13}(t))/2 = I_{1-23}(t)/2. \tag{2.3.5.2}$$

The relations above allow us to interpret the different dynamical behaviors of the bipartite entropies $S_{13-2}(t)$ and $S_{12-3}(t)$ as follows.

For values of $J/p < 0.35$ it holds that $\overline{S_{13-2}(t)} > \overline{S_{12-3}}(t) \implies \overline{I_{12}(t)} > \overline{I_{13}(t)}$. This inequality agrees well with physical intuition. When a local interaction dominates the dynamics low information is shared between the spins, and the information shared by adjacent spins is slightly larger than the information shared between non-adjacent spins. As the interaction parameter increases the average mutual information between the non-adjacent permutable spins 1-3 increases faster than the average mutual information between adjacent spins 1-2, 2-3. When the local and interaction parameters have equal magnitude, $J/p = 1$, the average $\overline{I_{13}(t)} \approx 0.9064$ is already much larger than the average $\overline{I_{12}(t)} \approx 0.6448$. Remarkably, this is the first point such that the mutual information I_{1-23}, which in words is the information shared by the first spin with the rest of the chain, reaches values higher than 1.999 in the dynamics. As J/p continues increasing so does $\overline{I_{13}(t)}$, while $\overline{I_{12}(t)}$ keeps growing but very slowly until reaching its maximum at $J/p \approx 2.19$, and then starts converging toward its asymptotic value of 0.6574. For large values of $J/p > 4.68$ the average $\overline{I_{13}(t)}$ continues growing but insignificantly and it stabilizes around $\overline{I_{13}(t)} \approx 1.024$.

As it can be seen from the long time evolution of $\overline{S_{12-3}(t)} = I_{1-23}(t)/2$, shown in the lower panels of figure 2.11, as more time passes the average amount of information shared by the non-adjacent permutable spins 1 and 3 increases, while the average of information shared between adjacent spins remains stable. We conjecture that in much larger chains this behavior will be observable only in the permutable spins near the middle point of the chain due to the Lieb-Robinson bound [64]. Nonetheless, further exploration into progressively larger chains is needed to reach more definitive conclusions.

Chapter 3

Further outlook

We believe that our work opens an opportunity to study three different very interesting problems. We first ask, how will the environment of the system affect its time scales? As in the intermediate-regime the Poincare recurrences times are within experimental possibilities we believe it should be possible to determine how does the environment affect the returning times to the initial state of the system. A related question can be formulated in terms of entropies or mutual information. As we showed the mutual information between the non-adjacent spins 1-3 largely increases with time, will this be the same in an open system? it will greatly decrease, increase or remain the same with the influence of the environment? will the parity symmetry continue dominating the distribution of information? will the time averages of bipartite entropies still be adequate order parameters?

A second research pathway that we identify remains in the domain of closed quantum systems. In this category we identify yet another two different problems of interest. The first one is the obvious extension to larger chains with the same model. As we have identified signatures of a DQPT in the finite-chain the natural question is, will this signatures remain for larger chains? will the same four dynamical regimes that we have defined continue appearing? A study similar to the one we did here and the one done in [36] is, in our opinion, of great interest.

The second research pathway within the framework of closed systems is related to the phase-diagram of the XXZ-spin-1 model studied in [35]. Due to the time-reversibility of unitary dynamics we believe that the emerging dynamics following the same protocol we used here, but with positive anisotropy and interaction terms, will give similar results. In the phase diagram of the model this would be a quench from a large-D phase not to another phase of the model, but rather to a transition zone of it between two other phases. Therefore, we propose to study the quench dynamics emerging from the initial state that we used here with the following Hamiltonian

$$H = \hbar p \sum_i (\hat{S}_i^z)^2 + \hbar \sum_{\langle i,j \rangle} \Big[J(\hat{S}_i^x \hat{S}_j^x + \hat{S}_i^y \hat{S}_j^y) + \pm \delta J_z (\hat{S}_i^z \hat{S}_j^z) \Big]. \tag{3.0.0.1}$$

As is highly likely that in the finite case with $J_z = 0$ there will be signatures of a DQPT, we ask: will any value of J_z break this signatures? or there is a range either positive, negative or both for which the signatures are conserved? We believe that a systematic study of these quench dynamics from the large-D phase towards the XY and Haldane phases near the transition line between them will help bring light on the connection between DQPT and equilibrium phase-transitions. We emphasize that our results are preliminar and a first step towards this direction is a numerical study of the emerging dynamics with both positive interaction terms and positive anisotropy.

Conclusions

In this work we have studied the out of equilibrium emerging dynamics of a XY-spin-1 chain with single-ion anisotropy following a protocol of quantum quench. We have found that with the proposed model it is possible to obtain maximally entangled pairs of spin-1 systems starting from a completely separable state. We have determine signatures of a dynamical quantum phase transition around the point $J/p \approx 1.66$ in the trimer case (i.e. $N = 3$). In distinction to what happened in a a recent study on the out of equilibrium dynamics of the 1D-TFIM, where the non-analicities of the rate-function appeared only in discrete values of the quench parameters [38], the non-analicities in the rate function in our spin-1 model appear for all values of $J/p > 1.66$.

Our results show that determining the times at which finite-size effects dominate the dynamics, throghout the whole spectrum of the quench parameters, is fundamental to get the maximum physical information from time average quantities such as two-point spin-z correlations functions and bipartite entropies. We also determined that the time average over Poincare recurrence times of bipartite entropies are adequate order parameters, and provide a more complete and richer classification of the dynamics than the time average of the two-point spin-z correlation functions.

We analyzed the mutual information averages between the different spins in the case $N = 3$. This initial analysis indicates that when the interaction among spins is large enough in comparison to the local anisotropy, the mutual information between the permutable spins is larger than the mutual information between adjacent spins. However, this requires further exploration into larger chains.

Bibliography

1. Feynman, R. P. in *Feynman and Computation* 6/7, 133–153 (International Journal of Theoretical Physics, 1982).
2. Georgescu, I., Ashhab, S. & Nori, F. Quantum simulation. *Reviews of Modern Physics* **86,** 153–185 (Mar. 2014).
3. Cao, Y. *et al.* Quantum Chemistry in the Age of Quantum Computing. *Chemical Reviews* **119,** 10856–10915 (Aug. 2019).
4. Cirac, J. I. & Zoller, P. Goals and opportunities in quantum simulation. *Nature Physics* **8,** 264–266 (Apr. 2012).
5. Preskill, J. Quantum Computing in the NISQ era and beyond. *Quantum* **2,** 79 (Aug. 2018).
6. Blais, A., Huang, R.-S., Wallraff, A., Girvin, S. M. & Schoelkopf, R. J. Cavity quantum electrodynamics for superconducting electrical circuits: An architecture for quantum computation. *Physical Review A* **69** (June 2004).
7. Roushan, P. *et al.* Spectroscopic signatures of localization with interacting photons in superconducting qubits. *Science* **358,** 1175–1179 (Nov. 2017).
8. Ma, R. *et al.* A dissipatively stabilized Mott insulator of photons. *Nature* **566,** 51–57 (Feb. 2019).
9. Zha, C. *et al.* Ergodic-Localized Junctions in a Periodically Driven Spin Chain. *Physical Review Letters* **125** (Oct. 2020).
10. Blatt, R. & Roos, C. F. Quantum simulations with trapped ions. *Nature Physics* **8,** 277–284 (Apr. 2012).
11. Bernien, H. *et al.* Probing many-body dynamics on a 51-atom quantum simulator. *Nature* **551,** 579–584 (Nov. 2017).
12. Greiner, M., Mandel, O., Esslinger, T., Hänsch, T. W. & Bloch, I. Quantum phase transition from a superfluid to a Mott insulator in a gas of ultracold atoms. *Nature* **415,** 39–44 (Jan. 2002).
13. Bloch, I., Dalibard, J. & Zwerger, W. Many-body physics with ultracold gases. *Reviews of Modern Physics* **80,** 885–964 (July 2008).
14. Orús, R. Tensor networks for complex quantum systems. *Nature Reviews Physics* **1,** 538–550 (Aug. 2019).
15. Polkovnikov, A., Sengupta, K., Silva, A. & Vengalattore, M. Colloquium: Nonequilibrium dynamics of closed interacting quantum systems. *Reviews of Modern Physics* **83,** 863–883 (Aug. 2011).
16. Bojan Zunkovic, M. H. M. K. & Silva, A. Dynamical Quantum Phase Transitions in Spin Chains with Long-Range Interactions, Merging Different Concepts of Nonequilibrium Criticality. *Physical Review Letters* (2018).
17. Greentree, A. D., Tahan, C., Cole, J. H. & Hollenberg, L. C. L. Quantum phase transitions of light. *Nature Physics* **2,** 856–861 (Nov. 2006).
18. Hartmann, M. J., Brandão, F. G. S. L. & Plenio, M. B. Strongly interacting polaritons in coupled arrays of cavities. *Nature Physics* **2,** 849–855 (Nov. 2006).
19. Fisher, M. P. A., Weichman, P. B., Grinstein, G. & Fisher, D. S. Boson localization and the superfluid-insulator transition. *Physical Review B* **40,** 546–570 (July 1989).
20. Peña, R., Torres, F. & Romero, G. Dynamical dimerization phase in Jaynes–Cummings lattices. *New Journal of Physics* **22,** 033034 (Mar. 2020).
21. Einstein, A., Podolsky, B. & Rosen, N. Can Quantum-Mechanical Description of Physical Reality Be Considered Complete? *Physical Review* **47,** 777–780 (May 1935).

22. Bell, J. S. On the einstein podolsky rosen paradox. *Physics Physique Fizika* **1,** 195 (1964).
23. Aspect, A., Dalibard, J. & Roger, G. Experimental Test of Bell's Inequalities Using Time- Varying Analyzers. *Physical Review Letters* **49,** 1804–1807 (Dec. 1982).
24. Nielsen, M. A. & Chuang, I. L. *Quantum Computation and Quantum Information* (Cambridge University Press, 2010).
25. Plenio, M. B. & Virmani, S. S. An introduction to entanglement theory. *Quantum information and coherence,* 173–209 (2014).
26. Läuchli, A. M. & Kollath, C. Spreading of correlations and entanglement after a quench in the one-dimensional Bose–Hubbard model. *Journal of Statistical Mechanics: Theory and Experiment* **2008,** P05018 (May 2008).
27. Mukherjee, V., Divakaran, U., Dutta, A. & Sen, D. Quenching dynamics of a quantumXYspin-12chain in a transverse field. *Physical Review B* **76,** 174303 (Nov. 2007).
28. Ciliberti, L., Canosa, N. & Rossignoli, R. Discord and information deficit in theXXchain. *Physical Review A* **88,** 012119 (July 2013).
29. Dillenschneider, R. Quantum discord and quantum phase transition in spin chains. *Physical Review B* **78,** 224413 (Dec. 2008).
30. Sarandy, M. S. Classical correlation and quantum discord in critical systems. *Physical Review A* **80,** 022108 (Aug. 2009).
31. Maziero, J., Guzman, H. C., Céleri, L. C., Sarandy, M. S. & Serra, R. M. Quantum and classical thermal correlations in theXYspin-12chain. *Physical Review A* **82,** 012106 (July 2010).
32. Canovi, E., Ercolessi, E., Naldesi, P., Taddia, L. & Vodola, D. Dynamics of entanglement entropy and entanglement spectrum crossing a quantum phase transition. *Physical Review B* **89,** 104303 (Mar. 2014).
33. Chung, W. C., de Hond, J., Xiang, J., Cruz-Colón, E. & Ketterle, W. Tunable Single-Ion Anisotropy in Spin-1 Models Realized with Ultracold Atoms. *Physical Review Letters* **126,** 163203 (Apr. 2021).
34. Heyl, M. Dynamical quantum phase transitions: a review. *Reports on Progress in Physics* **81,** 054001 (Apr. 2018).
35. Chen, W., Hida, K. & Sanctuary, B. C. Ground-state phase diagram ofS=1XXZchains with uniaxial single-ion-type anisotropy. *Physical Review B* **67,** 104401 (Mar. 2003).
36. Hagymási, I., Hubig, C., Legeza, Ö. & Schollwöck, U. Dynamical Topological Quantum Phase Transitions in Nonintegrable Models. *Physical Review Letters* **122,** 250601 (June 2019).
37. Malvezzi, A. L. *et al.* Quantum correlations and coherence in spin-1 Heisenberg chains. *Physical Review B* **93,** 184428 (May 2016).
38. Zhou, B., Zeng, Y. & Chen, S. Exact zeros of the Loschmidt echo and quantum speed limit time for the dynamical quantum phase transition in finite-size systems. *Physical Review B* **104,** 094311 (Sept. 2021).
39. Tasaki, H. *Physics and mathematics of quantum many-body systems* (Springer Nature, 2020).
40. Harris, C. R. *et al.* Array programming with NumPy. **585,** 357–362 (Sept. 2020).
41. Ballentine, L. E. *Quantum mechanics: a modern development* (World Scientific Publishing Company, 2014).
42. Van Rossum, G. *The Python Library Reference, release 3.8.2* (Python Software Foundation, 2020).
43. Jones, E., Oliphant, T., Peterson, P., *et al. SciPy: Open source scientific tools for Python* 2001–. `http://www.scipy.org/`.
44. Shannon, C. E. A mathematical theory of communication. *The Bell system technical journal* **27,** 379–423 (1948).
45. Breuer, H.-P., Petruccione, F., *et al. The theory of open quantum systems* (Oxford University Press on Demand, 2002).
46. Cover, T. M. *Elements of information theory* (John Wiley & Sons, 1999).
47. Wehrl, A. General properties of entropy. *Reviews of Modern Physics* **50,** 221 (1978).
48. Donald, M. J., Horodecki, M. & Rudolph, O. The uniqueness theorem for entanglement measures. *Journal of Mathematical Physics* **43,** 4252–4272 (Sept. 2002).
49. Ollivier, H. & Zurek, W. H. Quantum Discord: A Measure of the Quantumness of Correlations. *Physical Review Letters* **88,** 017901 (Dec. 2001).
50. Datta, A. A Condition for the Nullity of Quantum Discord. arXiv: `1003.5256 [quant-ph]` (Mar. 2010).

51. Zurek, W. H. Quantum discord and Maxwell's demons. *Physical Review A* **67,** 012320 (Jan. 2003).
52. Eisert, J., Cramer, M. & Plenio, M. B. Colloquium: Area laws for the entanglement entropy. *Reviews of modern physics* **82,** 277 (2010).
53. Islam, R. *et al.* Measuring entanglement entropy in a quantum many-body system. *Nature* **528,** 77–83 (2015).
54. Singh, R., Bardarson, J. H. & Pollmann, F. Signatures of the many-body localization transition in the dynamics of entanglement and bipartite fluctuations. *New Journal of Physics* **18,** 023046 (2016).
55. Henderson, L. & Vedral, V. Classical, quantum and total correlations. *Journal of Physics A: Mathematical and General* **34,** 6899–6905 (Aug. 2001).
56. Modi, K., Brodutch, A., Cable, H., Paterek, T. & Vedral, V. The classical-quantum boundary for correlations: Discord and related measures. *Reviews of Modern Physics* **84,** 1655–1707 (Nov. 2012).
57. Werlang, T. & Rigolin, G. Thermal and magnetic quantum discord in Heisenberg models. *Physical Review A* **81,** 044101 (Apr. 2010).
58. Werlang, T., Trippe, C., Ribeiro, G. A. P. & Rigolin, G. Quantum Correlations in Spin Chains at Finite Temperatures and Quantum Phase Transitions. *Physical Review Letters* **105,** 095702 (Aug. 2010).
59. Galve, F., Giorgi, G. L. & Zambrini, R. Orthogonal measurements are almost sufficient for quantum discord of two qubits. **96,** 40005 (Nov. 2011).
60. Heyl, M., Polkovnikov, A. & Kehrein, S. Dynamical Quantum Phase Transitions in the Transverse-Field Ising Model. *Physical Review Letters* **110** (Mar. 2013).
61. Sciolla, B. & Biroli, G. Quantum Quenches and Off-Equilibrium Dynamical Transition in the Infinite-Dimensional Bose-Hubbard Model. *Physical Review Letters* **105,** 220401 (Nov. 2010).
62. Oganesyan, V. & Huse, D. A. Localization of interacting fermions at high temperature. *Physical Review B* **75,** 155111 (Apr. 2007).
63. Mirkin, N. & Wisniacki, D. Quantum chaos, equilibration, and control in extremely short spin chains. *Physical Review E* **103,** L020201 (2021).
64. Lieb, E. H. & Robinson, D. W. in *Statistical Mechanics* 425–431 (Springer Berlin Heidelberg, 1972).

Appendix A

Proofs

Proof $\left[\hat{S}^z, H\right] = 0$**.** Expanding the commutator and using the canonical commutation relations directly follows that

$$\begin{aligned}\left[\hat{S}_z, \hat{H}\right] &= -p\sum_{i=1}^{N}\left[\hat{S}_i^z, (\hat{S}_i^z)^2\right] - J\sum_{i=1}^{N}\left[\hat{S}_i^z, \sum_{j=1}^{N-1}\hat{S}_j^x\hat{S}_{j+1}^x + \hat{S}_j^y\hat{S}_{j+1}^y\right] \\ &= -iJ\Big\{\hat{S}_1^y\hat{S}_2^x - \hat{S}_1^x\hat{S}_2^y + \hat{S}_{N-1}^x\hat{S}_N^y - \hat{S}_{N-1}^y\hat{S}_N^x \\ &\quad + \sum_{i=2}^{N-1}\hat{S}_i^y\hat{S}_{i+1}^x - \hat{S}_i^x\hat{S}_{i+1}^y + \hat{S}_{i-1}^x\hat{S}_i^y - \hat{S}_{i-1}^y\hat{S}_i^x\Big\} = 0. \qquad \blacksquare\end{aligned} \tag{A.1}$$

Proof $\left[\hat{S}^2, H\right] = 0$**.** Note the following commutators

$$\begin{aligned}\left[(\hat{S}_i^x)^2, \hat{S}_i^y\right] &= i\Big\{\hat{S}_i^x, \hat{S}_i^z\Big\}, \qquad \left[(\hat{S}_i^y)^2, \hat{S}_i^x\right] = -i\Big\{\hat{S}_i^y, \hat{S}_i^z\Big\}, \\ \left[(\hat{S}_i^z)^2, \hat{S}_i^x\right] &= i\Big\{\hat{S}_i^y, \hat{S}_i^z\Big\}, \qquad \left[(\hat{S}_i^z)^2, \hat{S}_i^y\right] = -i\Big\{\hat{S}_i^x, \hat{S}_i^z\Big\}.\end{aligned} \tag{A.2}$$

With them is direct to obtain the commutator of each $(\hat{S}^\alpha)^2$ with the interaction part of the Hamiltonian:

$$\begin{aligned}\left[(\hat{S}^x)^2, \sum_{j=1}^{N-1}\hat{S}_j^x\hat{S}_{j+1}^x + \hat{S}_j^y\hat{S}_{j+1}^y\right] &= \sum_{i=2}^{N-1}\Big(i\Big\{\hat{S}_i^x, \hat{S}_i^z\Big\}\hat{S}_{i+1}^y + i\hat{S}_{i-1}^y\Big\{\hat{S}_i^x, \hat{S}_i^z\Big\}\Big) \\ &\quad + i\Big\{\hat{S}_1^x, \hat{S}_1^z\Big\}\hat{S}_2^y + i\hat{S}_{N-1}^y\Big\{\hat{S}_N^x, \hat{S}_N^z\Big\}\end{aligned} \tag{A.3}$$

$$\begin{aligned}\left[(\hat{S}^y)^2, \sum_{j=1}^{N-1}\hat{S}_j^x\hat{S}_{j+1}^x + \hat{S}_j^y\hat{S}_{j+1}^y\right] &= \sum_{i=2}^{N-1}\Big(-i\Big\{\hat{S}_i^y, \hat{S}_i^z\Big\}\hat{S}_{i+1}^x - i\hat{S}_{i-1}^x\Big\{\hat{S}_i^y, \hat{S}_i^z\Big\}\Big) \\ &\quad - i\Big\{\hat{S}_1^y, \hat{S}_1^z\Big\}\hat{S}_2^x - i\hat{S}_{N-1}^x\Big\{\hat{S}_N^y, \hat{S}_N^z\Big\}\end{aligned} \tag{A.4}$$

$$\begin{aligned}\left[(\hat{S}^z)^2, \sum_{j=1}^{N-1}\hat{S}_j^x\hat{S}_{j+1}^x + \hat{S}_j^y\hat{S}_{j+1}^y\right] &= \sum_{i=2}^{N-1}\Big(i\Big\{\hat{S}_i^y, \hat{S}_i^z\Big\}\hat{S}_{i+1}^x + i\hat{S}_{i-1}^x\Big\{\hat{S}_i^y, \hat{S}_i^z\Big\} - i\Big\{\hat{S}_i^x, \hat{S}_i^z\Big\}\hat{S}_{i+1}^y - i\hat{S}_{i-1}^y\Big\{\hat{S}_i^x, \hat{S}_i^z\Big\}\Big) \\ &\quad i\Big\{\hat{S}_1^y, \hat{S}_1^z\Big\}\hat{S}_2^x + i\hat{S}_{N-1}^x\Big\{\hat{S}_N^y, \hat{S}_N^z\Big\} - i\Big\{\hat{S}_1^x, \hat{S}_1^z\Big\}\hat{S}_2^y - i\hat{S}_{N-1}^y\Big\{\hat{S}_N^x, \hat{S}_N^z\Big\}.\end{aligned} \tag{A.5}$$

Collecting terms it follows that $\left[\hat{S}^2, \sum_{j=1}^{N-1} \hat{S}_j^x \hat{S}_{j+1}^x + \hat{S}_j^y \hat{S}_{j+1}^y\right] = 0$. Also follows that in general $\left[\hat{S}^2, \sum_{\langle i,j\rangle} S_i^\alpha S_j^\alpha\right] = 0$ for $\alpha = x, y, z$ and $\langle i, j\rangle$ any set of pair to pair interactions. In words this means that the total spin $\hat{S}^2$ is always conserved by pair-to-pair spin interactions.

For the commutator with the local terms of the Hamiltonian note the following

$$\begin{aligned}\Big[(\hat{S}_i^x)^2, (\hat{S}_i^z)^2\Big] &= -i\Big(\hat{S}_i^x\Big\{\hat{S}_i^z, \hat{S}_i^y\Big\} + \Big\{\hat{S}_i^z, \hat{S}_i^y\Big\}\hat{S}_i^x\Big).\\ \Big[(\hat{S}_i^y)^2, (\hat{S}_i^z)^2\Big] &= i\Big(\hat{S}_i^y\Big\{\hat{S}_i^z, \hat{S}_i^x\Big\} + \Big\{\hat{S}_i^z, \hat{S}_i^x\Big\}\hat{S}_i^y\Big).\end{aligned} \tag{A.6}$$

When summed give

$$\begin{aligned}\Big[(\hat{S}_i^x)^2 + (\hat{S}_i^y)^2, (\hat{S}_i^z)^2\Big] &= i\Big(\hat{S}_i^y\hat{S}_i^x\hat{S}_i^z - \hat{S}_i^x\hat{S}_i^y\hat{S}_i^z + \hat{S}_i^z\hat{S}_i^x\hat{S}_i^y - \hat{S}_i^z\hat{S}_i^y\hat{S}_i^x\Big)\\ &= i\Big(\Big[\hat{S}_i^y, \hat{S}_i^x\Big]\hat{S}_i^z + \hat{S}_i^z\Big[\hat{S}_i^x, \hat{S}_i^y\Big]\Big)\\ &= 0.\end{aligned} \tag{A.7}$$

And therefore $\Big[\hat{S}^2, H\Big] = 0$. ■

Proof of $U(1)$ symmetry

$$(U_z^\theta)^\dagger H U_z^\theta = H, \quad \text{with} \quad U_z^\theta \equiv \exp\Big(-i\theta\hat{S}_z\Big). \tag{A.8}$$

Explicitly developing the transformation

$$\begin{aligned}(U_z^\theta)^\dagger H U_z^\theta = &\prod_{i=1}^N \exp\Big(i\theta\hat{S}_i^z\Big)\left(\sum_{k=1}^N (\hat{S}_k^z)^2\right)\prod_{j=1}^N \exp\Big(-i\theta\hat{S}_j^z\Big)\\ &+ \prod_{i=1}^N \exp\Big(i\theta\hat{S}_i^z\Big)\left(\sum_{k=1}^{N-1} \hat{S}_k^x\hat{S}_{k+1}^x + \hat{S}_k^y\hat{S}_{k+1}^y\right)\prod_{j=1}^N \exp\Big(-i\theta\hat{S}_j^z\Big),\end{aligned} \tag{A.9}$$

Is clear that it suffices to show that

$$\exp\Big(i\theta\hat{S}_k^z\Big)\Big((\hat{S}_k^z)^2\Big)\exp\Big(-i\theta\hat{S}_k^z\Big) = (\hat{S}_k^z)^2; \tag{A.10}$$

$$\exp\Big(i\theta\hat{S}_k^z\Big)\exp\Big(i\theta\hat{S}_{k+1}^z\Big)\Big(\hat{S}_k^x\hat{S}_{k+1}^x + \hat{S}_k^y\hat{S}_{k+1}^y\Big)\exp\Big(-i\theta\hat{S}_k^z\Big)\exp\Big(i\theta\hat{S}_{k+1}^z\Big) = \hat{S}_k^x\hat{S}_{k+1}^x + \hat{S}_k^y\hat{S}_{k+1}^y. \tag{A.11}$$

The first equality A.10 follows immediately from the known identity

$$\exp\Big(\hat{A}\Big)f(\hat{B})\exp\Big(-\hat{A}\Big) = f\Big(\exp\Big(\hat{A}\Big)\hat{B}\exp\Big(-\hat{A}\Big)\Big). \tag{A.12}$$

For A.11 one expands the left-side using the known series expansion

$$\exp\Big(\hat{A}\Big)\hat{B}\exp\Big(-\hat{A}\Big) = \hat{B} + \Big[\hat{A}, \hat{B}\Big] + \frac{1}{2!}\Big[\hat{A}, \Big[\hat{A}, \hat{B}\Big]\Big] + \cdots \equiv \sum_{n=0}^{\infty}\mathcal{C}_n(\hat{A}, \hat{B}). \tag{A.13}$$

Using the canonical commutation relations one directly obtains

$$\mathcal{C}_n(i\theta\hat{S}_k^z, \hat{S}_k^x) = \begin{cases}(-1)^{n/2}\frac{\theta^n}{n!}\hat{S}_k^x & \text{for even} \quad n\\ (-1)^{(n+1)/2}\frac{\theta^n}{n!}\hat{S}_k^y & \text{for odd} \quad n\end{cases} \tag{A.14}$$

$$\mathcal{C}_n(i\theta\hat{S}_k^z, \hat{S}_k^y) = \begin{cases}(-1)^{n/2}\frac{\theta^n}{n!}\hat{S}_k^y & \text{for even} \quad n\\ (-1)^{(n-1)/2}\frac{\theta^n}{n!}\hat{S}_k^x & \text{for odd} \quad n\end{cases} \tag{A.15}$$

From where

$$\exp\Big(i\theta\hat{S}_k^z\Big)\hat{S}_k^x\exp\Big(-i\theta\hat{S}_k^z\Big)=\cos\theta\hat{S}_k^x-\sin\theta\hat{S}_k^y. \tag{A.16}$$

$$\exp\Big(i\theta\hat{S}_k^z\Big)\hat{S}_k^y\exp\Big(-i\theta\hat{S}_k^z\Big)=\cos\theta\hat{S}_k^y+\sin\theta\hat{S}_k^x. \tag{A.17}$$

Therefore

$$\begin{aligned}&\exp\Big(i\theta\hat{S}_k^z\Big)\exp\Big(i\theta\hat{S}_{k+1}^z\Big)\Big(\hat{S}_k^x\hat{S}_{k+1}^x\Big)\exp\Big(-i\theta\hat{S}_k^z\Big)\exp\Big(i\theta\hat{S}_{k+1}^z\Big)\\&\qquad=\cos^2\theta\hat{S}_k^x\hat{S}_{k+1}^x+\sin^2\theta\hat{S}_k^y\hat{S}_{k+1}^y-\frac{\sin(2\theta)}{2}\Big(\hat{S}_k^x\hat{S}_{k+1}^y+\hat{S}_k^y\hat{S}_{k+1}^x\Big);\end{aligned} \tag{A.18}$$

$$\begin{aligned}&\exp\Big(i\theta\hat{S}_k^z\Big)\exp\Big(i\theta\hat{S}_{k+1}^z\Big)\Big(\hat{S}_k^y\hat{S}_{k+1}^y\Big)\exp\Big(-i\theta\hat{S}_k^z\Big)\exp\Big(i\theta\hat{S}_{k+1}^z\Big)\\&\qquad=\cos^2\theta\hat{S}_k^y\hat{S}_{k+1}^y+\sin^2\theta\hat{S}_k^x\hat{S}_{k+1}^x+\frac{\sin(2\theta)}{2}\Big(\hat{S}_k^x\hat{S}_{k+1}^y+\hat{S}_k^y\hat{S}_{k+1}^x\Big).\end{aligned} \tag{A.19}$$

Immediately follows that A.11 is true, and therefore A.8 is proven. ■

Proof of $[\Pi,H]=0$**.** Noting that

$$\Big[\Pi_j^i,\hat{S}_i^\alpha+\hat{S}_j^\alpha\Big]=\Big[\Pi_j^i,\hat{S}_i^\alpha\hat{S}_j^\alpha\Big]=\Big[\Pi_j^i,(\hat{S}_i^\alpha)^2+(\hat{S}_j^\alpha)^2\Big]=0\quad\text{with}\quad\alpha=x,y,z. \tag{A.20}$$

For even N Immediately follows that

$$\left[\Pi,\sum_{j=1}^{N}(\hat{S}_j^\alpha)^2\right]=\sum_{i=0}^{(N-2)/2}\left[\Pi_{N-i}^{i+1},(\hat{S}_{i+1}^\alpha)^2+(\hat{S}_{N-i}^\alpha)^2+\sum_{j=0,\neq(i+1,N-i)}^{N}(\hat{S}_j^\alpha)^2\right]=0. \tag{A.21}$$

And also

$$\begin{aligned}\left[\Pi,\sum_{j=1}^{N-1}\hat{S}_j^\alpha\hat{S}_{j+1}^\alpha\right]&=\sum_{i=1}^{N/2-2}\left[\Pi_{N-i}^{i+1},\hat{S}_i^\alpha\hat{S}_{i+1}^\alpha+\hat{S}_{i+1}^\alpha\hat{S}_{i+2}^\alpha+\hat{S}_{N-i}^\alpha\hat{S}_{N-i+1}^\alpha+\hat{S}_{N-i-1}^\alpha\hat{S}_{N-i}^\alpha+\sum_{j=0\neq i+1,N-i}^{N-1}\hat{S}_j^\alpha\hat{S}_{j+1}^\alpha\right]\\&\quad+\Big[\Pi_{N-1}^1,\hat{S}_1^\alpha\hat{S}_2^\alpha+\hat{S}_{N-1}^\alpha\hat{S}_N^\alpha\Big]+\Big[\Pi_{N/2+1}^{N/2},\hat{S}_{N/2-1}^\alpha\hat{S}_{N/2}^\alpha+\hat{S}_{N/2}^\alpha\hat{S}_{N/2+1}^\alpha+\hat{S}_{N/2+1}^\alpha\hat{S}_{N/2+2}^\alpha\Big]\\&=0.\end{aligned} \tag{A.22}$$

In the odd case the proof of the commutation with the local term is written in the same way as above. Explicitly writing the commutator with the interaction term

$$\begin{aligned}\left[\Pi,\sum_{j=1}^{N}\hat{S}_j^\alpha\hat{S}_{j+1}^\alpha\right]&=\sum_{i=1}^{(N-1)/2-2}\left[\Pi_{N-i}^{i+1},\hat{S}_i^\alpha\hat{S}_{i+1}^\alpha+\hat{S}_{i+1}^\alpha\hat{S}_{i+2}^\alpha+\hat{S}_{N-i}^\alpha\hat{S}_{N-i+1}^\alpha+\hat{S}_{N-i-1}^\alpha\hat{S}_{N-i}^\alpha+\sum_{j=0\neq i+1,N-i}^{N-1}\hat{S}_j^\alpha\hat{S}_{j+1}^\alpha\right]\\&\quad+\Big[\Pi_{N-1}^1,\hat{S}_1^\alpha\hat{S}_2^\alpha+\hat{S}_{N-1}^\alpha\hat{S}_N^\alpha\Big]\\&\quad+\Big[\Pi_{(N-1)/2}^{(N+3)/2},\hat{S}_{(N-3)/2}^\alpha\hat{S}_{(N-1)/2}^\alpha+\hat{S}_{(N-1)/2}^\alpha\hat{S}_{(N+1)/2}^\alpha+\hat{S}_{(N+1)/2}^\alpha\hat{S}_{(N+3)/2}^\alpha+\hat{S}_{(N+3)/2}^\alpha\hat{S}_{(N+5)/2}^\alpha\Big]\\&=0.\end{aligned} \tag{A.23}$$

And it is proven that $[\Pi,H]=0$. ■

Appendix B

Trimer Additional Results

Here we start discussing the connection between T_m and T_r with the eigenfrequencies of the system. T_m is a *'least common'* multiple of the system frequencies $T_m = l\Delta_{10} = m\Delta_{21}$. The times T_r also are near integer multiples of the frequencies, but in contrast to T_m, for $J/p > 1.00$ T_r continues growing quadratically with respect to J/p. In figure B.1 we plot both T_m and T_r as a function of $\log(J/p)$.

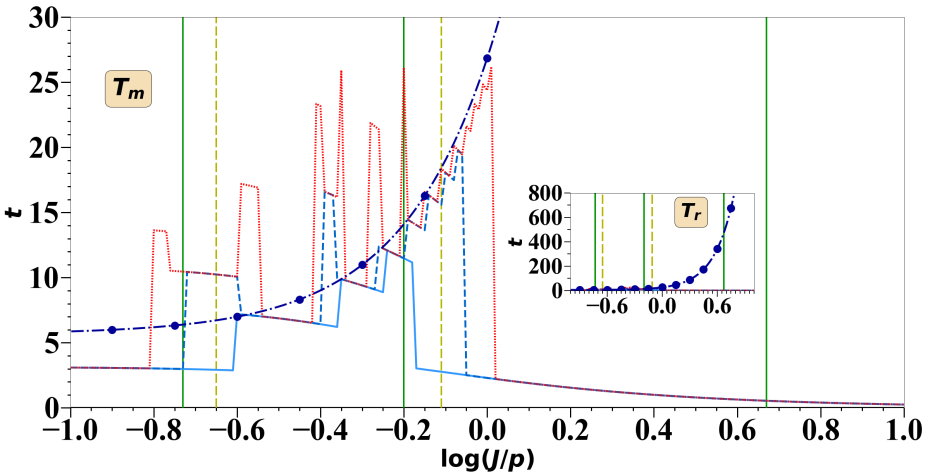

Figure B.1: Values of T_m and T_r in units of p^{-1} as a function of $\log(J/p)$. The $\log(J/p)$ is taken in base 10. The dotted line shows T_m as define in the main text. The dashed and solid lines show T_m defined as the time where the system reaches a fidelity $F_0(t) > 0.98, 0.95$ respectively. The line with the circle markers shows an exponential fit to the T_r times, manually found by determining the half-time recurrence point in which the system starts returning to the initial state for each value of $\log(J/p)$ between -0.20 and 1.70 with a step of 0.05. The time T_r grows in an approximate cuadratic form with respect to J/p.

In the left panel of figure B.2 we plot the values of the frequencies Δ_{10}, Δ_{21} as a function of $\log(J/p)$. In the limit $J/p \to 0$ $R_f \to 0$ due to the degeneracy of the ground state when $J = 0$. In this limit the dominant angular frequency is $\Delta_{21} \approx 2p$ from where the period of evolution will be close to π. This explains the values of T_m when $p >> J$ (shown in the figure B.1). Around $\log(J/p) = 0.8$ the angular frequency Δ_{10} becomes large enough to influence T_m shown by the first rise in the right panel of the figure B.2. In the intermediate regime R_f rapidly increases and the values of l, m increase by finite jumps between near integers values. The values of T_m shown in the figure B.1 naturally correlate to this pattern. The peaks as the one in $\log(J/p) = -0.2$ are mostly eliminated when a fidelity of 0.98 is put as a threshold to define T_m instead of

0.99. As $R_f \sim 1$ T_m approximately becomes $2T_{10} \approx 2T_{21} \approx T_{20}$. This explains the observed quasi-periodic evolution in the interaction dominant regime. In this regime $T_m \approx \pi/(\sqrt{6}J + 2ap)$ with $a \equiv p/3\sqrt{6}J$, which we obtained by applying second order perturbation-theory to the effective Hamiltonian.

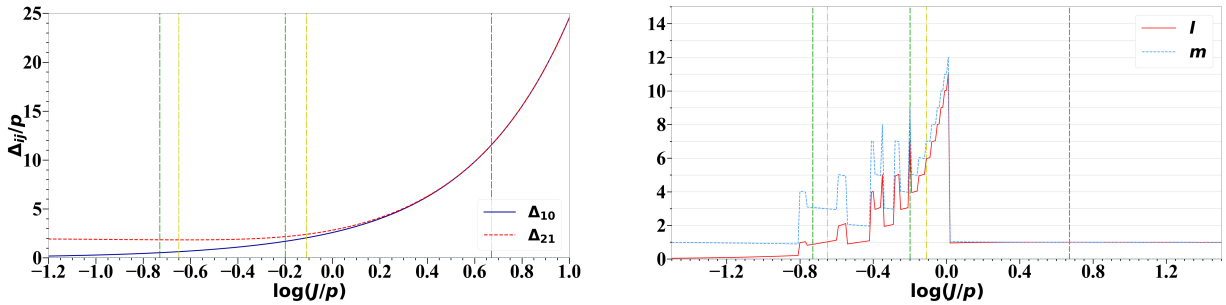

Figure B.2: The $\log(J/p)$ is taken in base 10. The left panel shows Δ_{10} and Δ_{21} in units of p as a function of $\log(J/p)$. The right panel shows the values of l, m when T_m is defined as in the main text. The peaks of the fidelity to determine T_m were located using the SCIPY built-in function find-peaks. In both panels the vertical dashed (dashdotted) lines are set at the inflection points of $\overline{S(t)_{13-2}}'$ ($\overline{S(t)_{12-3}}'$)

.

In figure B.3 we plot the weight of the effective Hamiltonian eigenstates in the accessible states $|\psi_1\rangle$ and $|\psi_2\rangle$. In the limit $J/p \to 0$ both states are linear combinations of the ground and first excited states each one with weight 1/2. In the intermediate-regime there is a *'mixing'* in the weights distribution. In the limit $J/p \to \infty$ $|\psi_1\rangle$ is a liner combination of the ground and most excited states each with weight 1/2, and $|\psi_2\rangle$ is a linear combination of all three eigenstates with a dominant weight of first-excited state $|E_1\rangle$ equal to 2/3. As the weights of the effective Hamiltonian eigenstates in the accessible states $|\psi_1\rangle$ and $|\psi_2\rangle$ are not equal to their weights in the initial state, the probability amplitudes $|\langle\psi_1|\psi(t)\rangle|^2$ and $|\langle\psi_2|\psi(t)\rangle|^2$ will never be one.

In the local-dominant regime $J/p < 0.22$ the system is always near the initial state and quasi-periodically returns to it completing a Poincare recurrence. When $J/p \sim 1.00$ the system oscillates without periodicity departing from the initial state, until reaching a minimal value of the fidelity before finite size effects dominate the dynamics and the system starts returning to the initial state completing a Poincare Recurrence. We show the long time evolution of $\mathcal{L}(t)$ for $J/p \approx 0.22, 1.00$ in the figure B.4.

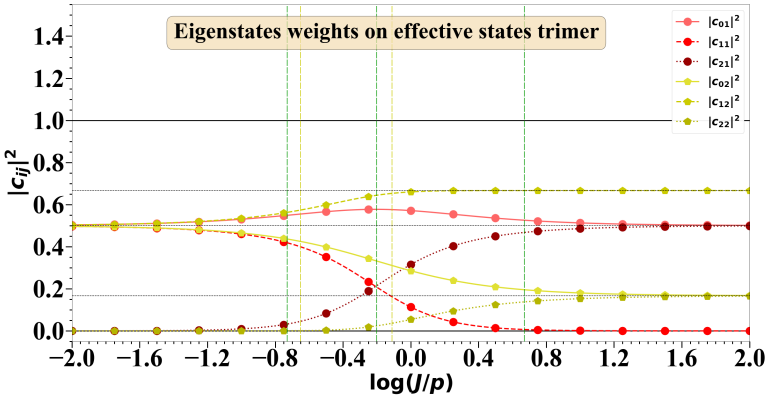

Figure B.3: Weights of the effective Hamiltonian eigenstates in the accessible states $|\psi_1\rangle$ and $|\psi_2\rangle$ as a function of $\log(J/p)$. The $\log(J/p)$ is taken in base 10.

The longitudinal spin alignment at time t reads

$$A = 2 - 2(|c_1(t)|^2 + |c_2(t)|^2) = 2|c_0(t)|^2. \tag{B.1}$$

Thus $A(t)$ evolves in a similar way as $\mathcal{L}(t)$ as shown in the main text in figures 2.8 and 2.7. By measuring $A(t)$ the Loschmidt echo $\mathcal{L}(t)$ will be indirectly measured and it will be possible to determined both the Poincare recurrence times T_r of the system for $J/p \sim 1$, and the lowest value of J/p at which the system reaches orthogonality (i.e. $\mathcal{L}(t) \approx 0 \rightarrow A(t) \approx 0$). For larger values of J/p the experimental values of T_r are too large and decoherence effects will dominate the dynamics. Nonetheless T_m gets shorter as J/p increases and its value can in principle be well determined by measuring $A(t)$. For larger chains the fidelity will not be directly measured by the longitudinal spin alignment, but both times T_r and T_m can be well detected as $A(t) \approx 2$ only when $\mathcal{L}(t) \approx 1$. Even when decoherence effects start to dominate the dynamics it should be possible to measure T_m and T_r as in general the only spin-eigenstate in which $A = 2$ is $|000\rangle \equiv |\psi_0\rangle$.

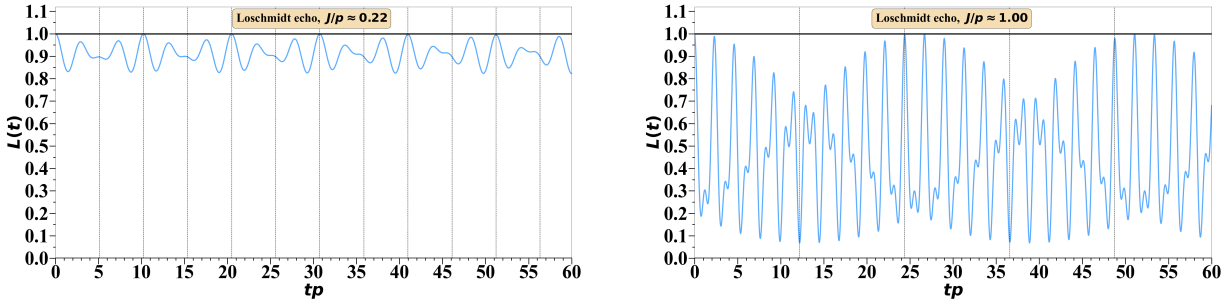

Figure B.4: The left panel shows $\mathcal{L}(t)$ for $\log(J/p) = -0.65 \rightarrow J/p \approx 0.22$. The right panel shows $\mathcal{L}(t)$ for $\log(J/p) = 0.00 \rightarrow J/p = 1.00$. The vertical dashed lines in both panels are set at integers multiples of $T_r/2$.

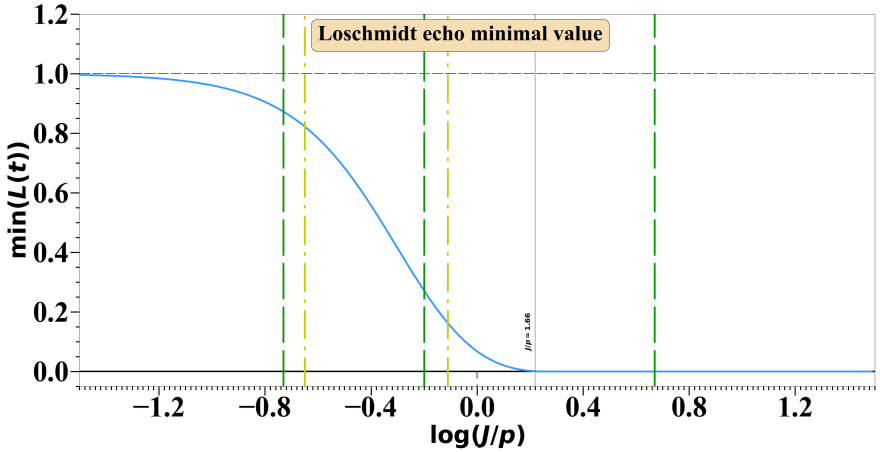

Figure B.5: Loschmidt echo minimal values reach in the dynamics as a function of $\log(J/p)$. The $\log(J/p)$ is taken in base 10. The minimum are shown for all values of $\log(J/p)$ between -1.6 and 1.6 with a step of 0.01.

The evolution of the spin-z correlations $C_{12}(t)$ and $C_{13}(t)$ for $J/p \sim 1$ clearly reflect the Poincare recurrences of the system as shown in the upper panels of figure B.6. Nonetheless, for longer values of J/p, $C_{12}(t)$ becomes almost completely quasi-periodic and the Poincare recurrences signatures are lost as we show in the lower panels of figure B.6. In contrast, in the evolution of $C_{13}(t)$ the Poincare recurrence signatures remain in the interaction-dominant regime, see the lower right panel of figure B.6.

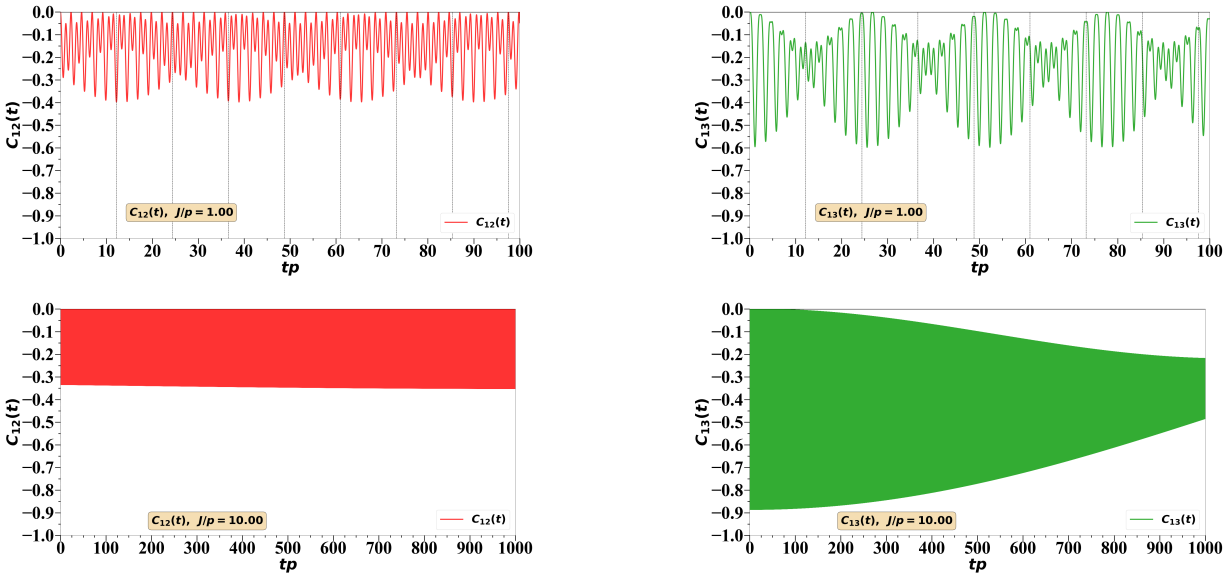

Figure B.6: Long time evolutions of the spin-z correlations for $\log(J/p) = 0.00, 1.00 \rightarrow J/p = 1.00, 10.00$. The vertical dashed lines are set at integer multiples of the half-recurrence time $T_r/2$. For $J/p \approx 10$ $T_r/2 \approx 1063\ p^{-1}$ not shown in the lower panels.

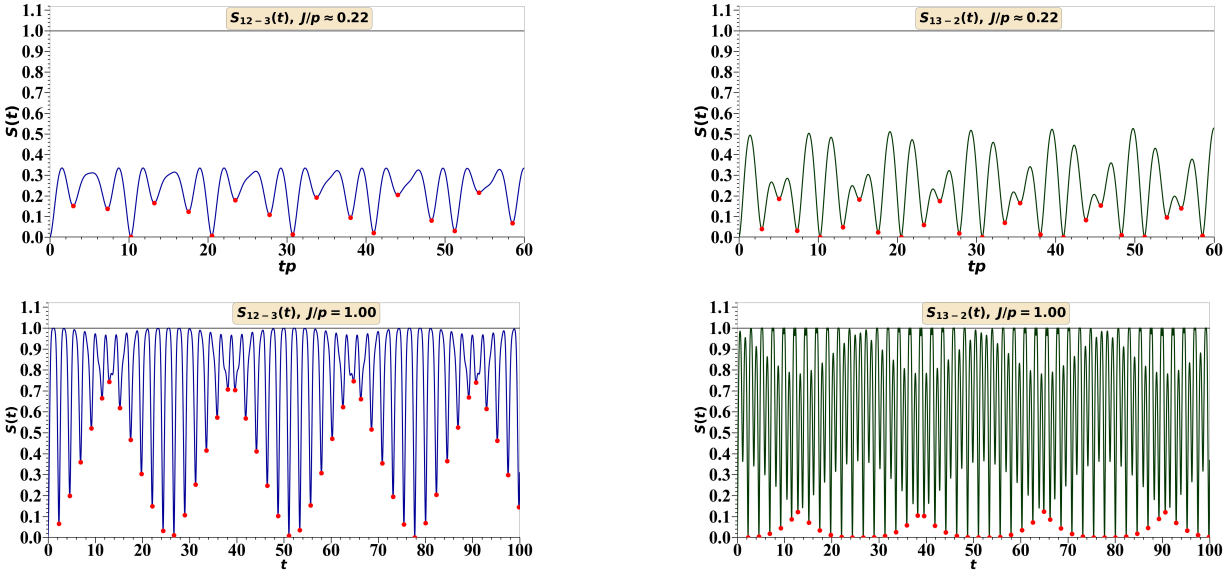

Figure B.7: The upper left (right) panel shows the long time evolution of $S_{12-3}(t)$ ($S_{13-2}(t)$) for $J/p \approx 0.22$. The lower left (right) panels show the long time evolution of $S_{12-3}(t)$ ($S_{13-2}(t)$) for $J/p = 1.00$.

In the figure B.7 we show the evolution of the bipartite entropies for $J/p = 1.00$. As commented in the main text this is the lowest value of J/p such that $S_{12-3}(t) > 0.999$ at some point in the dynamics. This means that the system reaches a state in which the information shared between the border spin 1 (or 3) with the rest of the chain is maximal.

In the figure B.8 we show the maximal values reach by the bipartite entropies in the dynamics. The lowest value of J/p in which the bipartite entropy $S_{13-2}(t)$ reaches values higher than 0.999 is $J/p \approx 0.78 \rightarrow \log(J/p) = -0.11$, which actually coincides with an inflection point of the first derivative of $S_{13} - 2(t)$. This

is most likely just a coincidence. Note that the maximal value reach by $S_{13-2}(t)$ is greater than the maximal value reach by $S_{12-3}(t)$ for $J/p < 1$.

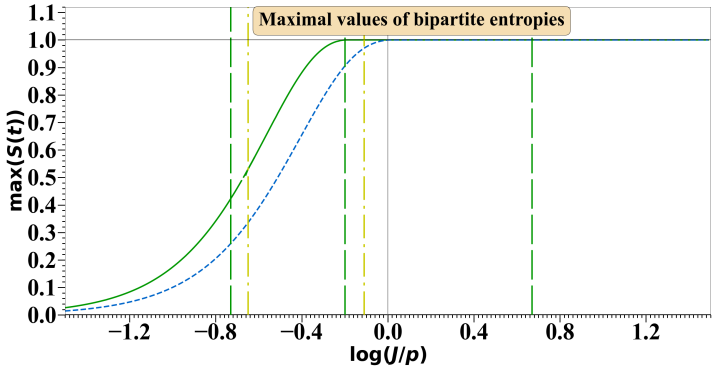

Figure B.8: Maximal values reach by the bipartite entropies in the evolution of the system. The $\log(J/p)$ is taken in base 10. The maximum are shown for $\log(J/p) \in (-1.5, 1.5)$ with a step of 0.01.

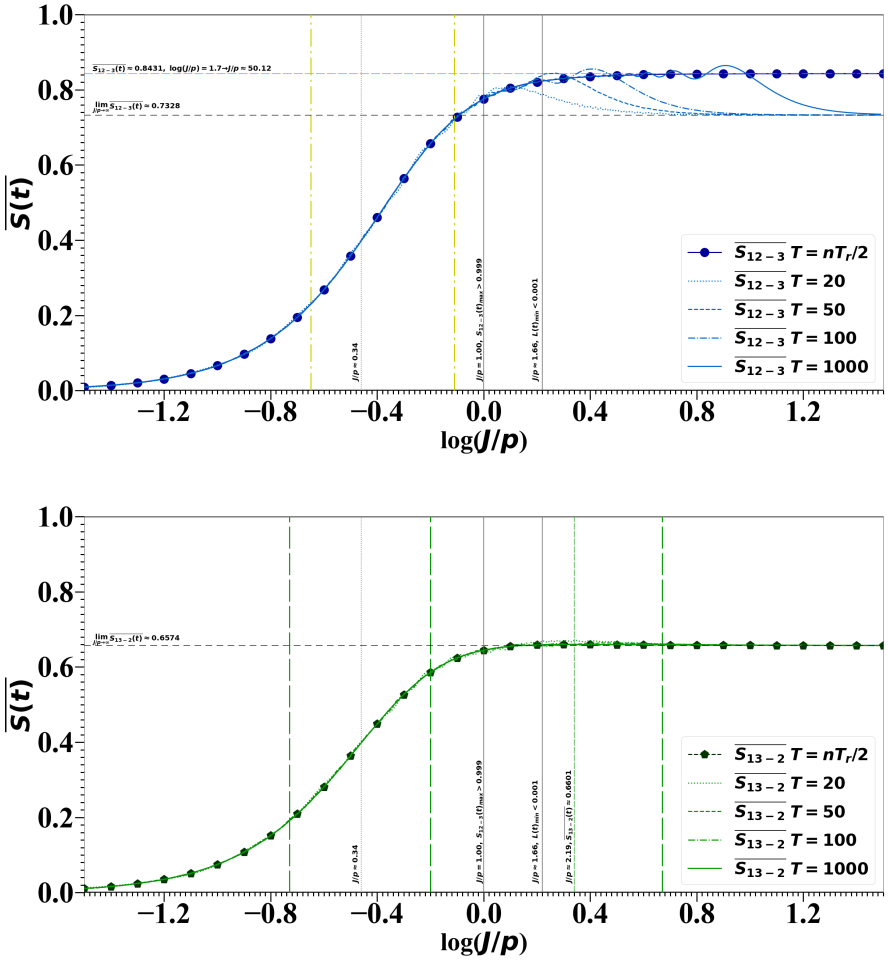

Figure B.9: Averages of the bipartite entropies for different fix values of T for all values of $\log(J/p)$ between $(-1.5, 1.5)$ with a step of 0.01.

As commented in the main text, when the bipartite entropies are averaged over fix values of T spurious non-physical oscillations appear throughout the J/p spectrum, even for large values of T. For increasing values of T the average entropies $\overline{S_{12-3}(t)}$ get closer to the average calculated over integer multiples of the half-recurrence times. For large values of J/p the curve for $T = 1000\ p^{-1}$ still converges towards the asymptotic value of the average due to the fact that the half-recurrence times become extremely large. For example for $\log(J/p) = 1.5\ T_r/2 \approx 10605\ p^{-1}$. Therefore, we conclude that although in the interaction-dominant regime the unitary evolution predicts an emerging dynamics different from the one that is obtained in the asymptotic limit $J/p \to \infty$, in any experimental situation the observed dynamics in this regime will resemble the one that can be obtained setting $p = 0, J > 0$, which has a period $T = \pi/\sqrt{6}J$. The experimental apparent period for a small but non-zero value of p should be given by $T_m \approx \pi/(\sqrt{6}J + 2ap)$ with $a \equiv p/3\sqrt{6}J$.